The Meteoritical Society

Meteoritics & Planetary Science 43, Nr 12, 2027–2048 (2008)
Abstract available online at http://meteoritics.org

Impact penetration of Europa's ice crust as a mechanism for formation of chaos terrain

Rónadh COX[1*], Lissa C. F. ONG[2, 4], Masahiko ARAKAWA[3], and Kate C. SCHEIDER[1]

[1]Department of Geosciences, Williams College, Williamstown, Massachusetts 01267, USA
[2]Departments of Astronomy and Physics, Williams College, Williamstown, Massachusetts 01267, USA
[3]Department of Earth and Planetary Physics, Nagoya University, Nagoya 464-8602, Japan
[4]Present address: Lunar and Planetary Laboratory, University of Arizona, 1629 E. University Blvd., Tucson, Arizona 85721, USA
[*]Corresponding author. E-mail: rcox@williams.edu

(Received 06 May 2008; revision accepted 23 June 2008)

Abstract–Ice thickness estimates and impactor dynamics indicate that some impacts must breach Europa's ice crust; and outcomes of impact experiments using ice-over-water targets range from simple craters to chaos-like destroyed zones, depending on impact energy and ice competence. First-order impacts—into thick ice or at low impact energy—produce craters. Second-order impacts punch through the ice, making holes that resemble raft-free chaos areas. Third-order impacts—into thinnest ice or at highest energy—produce large irregular raft-filled zones similar to platy chaos. Other evidence for an impact origin for chaos areas comes from the size-frequency distribution of chaos+craters on Europa, which matches the impact production functions of Ganymede and Callisto; and from small craters around the large chaos area Thera Macula, which decrease in average size and density per unit area as a function of distance from Thera's center. There are no tiny chaos areas and no craters >50 km diameter. This suggests that small impactors never penetrate, whereas large ones (ÜberPenetrators: >2.5 km diameter at average impact velocity) always do. Existence of both craters and chaos areas in the size range 2–40 km diameter points to spatial/temporal variation in crust thickness. But in this size range, craters are progressively outnumbered by chaos areas at larger diameters, suggesting that probability of penetration increases with increasing scale of impact. If chaos areas do represent impact sites, then Europa's surface is older than previously thought. The recalculated resurfacing age is 480 (−302/+960) Ma: greater than prior estimates, but still very young by solar system standards.

INTRODUCTION

Chaos formation is a major resurfacing mechanism that has affected more than 30% of Europa's surface (Riley et al. 2000). Pre-existing terrain is destroyed and replaced by rough-textured hummocky ground—interpreted as frozen liquid or slush (Greenberg et al. 1999; Collins et al. 2000)—often including relict blocks of the antecedent crust, which were broken and moved while the chaos matrix was fluid (Greeley et al. 1998; Spaun et al. 1998; Greenberg et al. 1999; Collins et al. 2000). Chaos terrain is enigmatic: there is no consensus as to what processes might create this geomorphology.

A major question is how to focus the energy needed to cause melting at or near Europa's surface, to breach the surface ice, and to generate the mixture of water, slush, and blocks that solidifies to form chaos terrain. Most work has focussed on internal energy and break-through from below, producing numerous models of how heat might be concentrated near Europa's solid surface. All of these models are disputed, however, and none is widely accepted (e.g., Greenberg et al. 1999; McKinnon 1999; Collins et al. 2000; Fagents et al. 2000; Riley et al. 2000; Figueredo et al. 2002; O'Brien et al. 2002; Goodman et al. 2004). But there is another possible energy source—impact from above—by which some subset of bolides arriving at Europa fully breach the crust, leaving behind a destroyed area filled with liquid slush and crustal detritus (Fig. 1). This external-energy model requires that the crust be thin enough to permit impact penetration.

Models for chaos formation must also address the size distribution of chaos areas. If chaos areas originate via impact, then the size-frequency distribution (SFD) of craters+chaos should correspond to a single monotonic function, which should represent the production function at

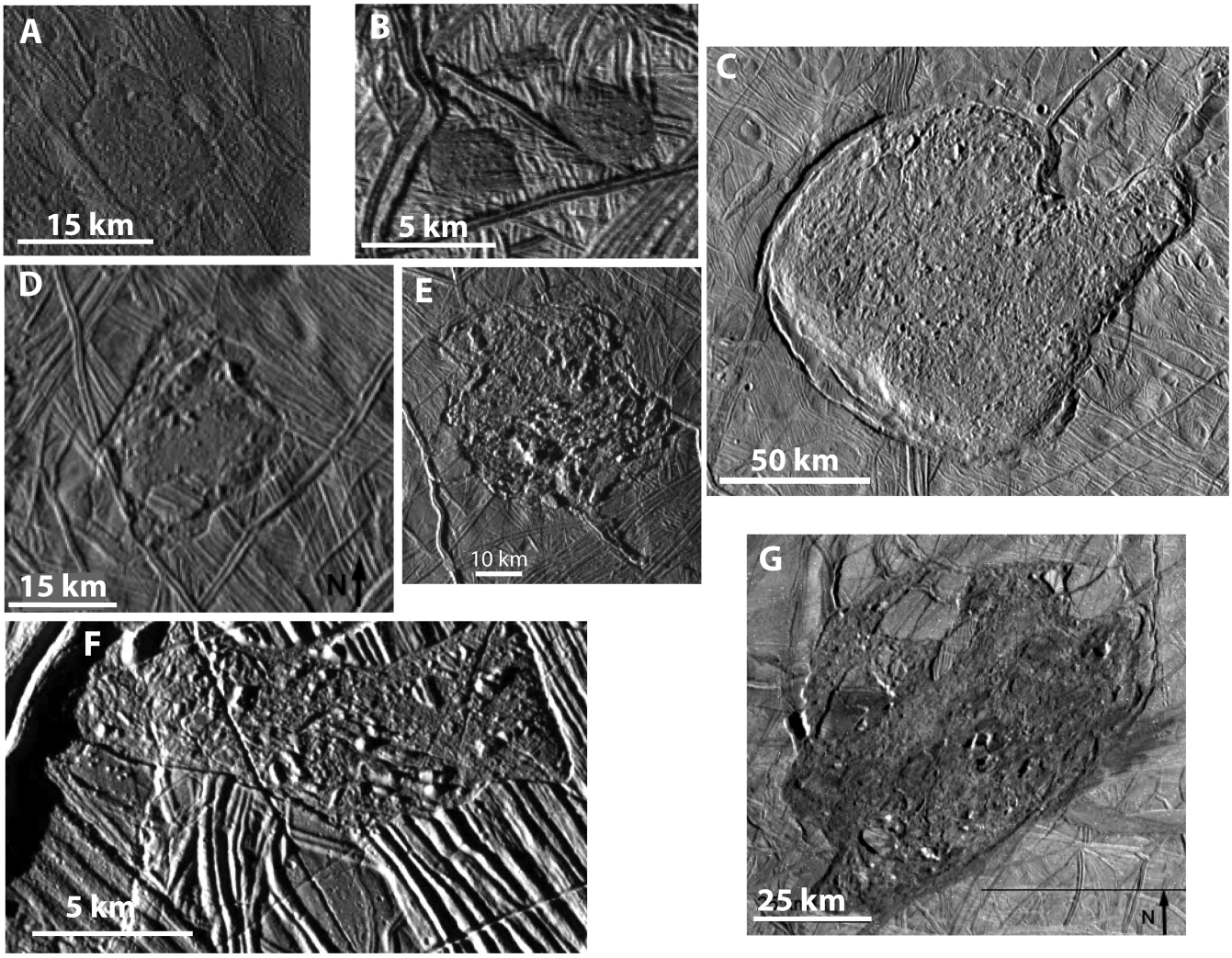

Fig. 1. Chaos areas showing impact-like morphology with equidimensional shapes, scarp-like and onlapping boundaries, and demolished interiors. The chaos material is refrozen slush that may have been impact melt and/or exposed sub-crustal liquid, and the blocks are pieces of crust broken from the edges of the hole and displaced toward the center. a) Narberth Chaos: smooth-outline chaos, image E6 5504 (near Pwyll; overprinted by Pwyll secondaries). b) Pair of small chaos, image E19 8726. c). Murias Chaos ("the Mitten"), images E15 4300 and 4326. d) Arran Chaos: angular chaos with some rafts near edge, image E15 4265. e) Rathmore Chaos: angular platy chaos, image E15 4313. f) Angular platy chaos, image E11 6700. The chaos area has been modified and fractured by subsequent tectonic activity. g) Thera Macula, images E17 4400, 4401, 4413, 4414. (a–c) are interpreted as second-order impacts, (d) as transitional between second- and third-order, and (e–g) as third-order impacts.

Europa. The production population at Europa is not known independently, because of the scanty crater record; but it is expected to match that measured at Ganymede and Callisto (Schenk et al. 2004).

The questions on which we will focus most closely, therefore, are geomorphologic. Is the Europan crust penetrable by impactors? To what extent do the sites of ice-penetrating impacts resemble chaos areas? Is there any evidence for secondary cratering around chaos areas? And does the combined size-frequency distribution of craters plus chaos areas on Europa match a production population? We address these questions with data from the literature, experiments and image analysis. First, literature analysis indicates that some subset of bolides arriving at Europa should be able to penetrate the crust. Second, impact experiments document both incipient- and penetrating-impact outcomes in ice over liquid, providing an initial model of the geomorphologic expression of deep impact through thin crust, and showing that such impacts produce the features of chaos. Third, in the one place on Europa that image resolution permits us to examine—the area around Thera Macula—small-crater abundances decrease radially away from the chaos area. Finally, measurements from Galileo images show that the size-frequency distribution of chaos plus craters, expressed as a unified population, does indeed match the production function at Ganymede and Callisto.

Terms and Definitions

We use "*solid-target impact*" to designate cases where the target is infinitely thick with respect to the bolide: i.e., classic crater-producing events. We use the term "*penetrating impact*" for events that fully puncture a solid layer through to an underlying liquid, leaving a gaping hole, with or without floating remnants of the fractured solid layer. Intermediate between these two end-members is "*incipient penetration*," where the impactor damages the crust sufficiently that underlying liquid seeps up to the surface, but no wide-open hole is produced. Based on the experiments reported here, we define "*first-order events*" as those that do not fully penetrate the ice layer (including both solid-target and incipient penetration impacts). "*Second-order events*" produce clean "*bullet holes*", and "*third-order events*" produce wide-field fragmentation of the target. Because the same impactor energy produces different results depending on ice thickness, we use "*equivalent-bolide feature*" to compare these outcomes. "*Impact intensity*" describes the magnitude of the event, and can be thought of as the relationship between the force of impact and the resistance of the ice layer. Impact intensity can be expressed as

$$\frac{E}{T \times \rho} \quad (1)$$

where E is impact energy, T is ice thickness, and ρ is ice density. For example, a low-energy impactor will have low intensity in a thick target, but might have high intensity if the ice is thin or weak. For a given impactor energy, the impact intensity will increase as ice thickness decreases. Finally, to facilitate comparison of chaos and crater sizes, we recast our chaos area measurements as "*equivalent circle diameter*" (ECD): i.e., the diameter of a circle with area equivalent to the measured chaos area.

To identify chaos areas, we used the criteria of Greenberg et al. (1999): abrupt transition from background, matrix texture similar to that of Conamara Chaos, and generally including rafts (which at small scale merge with the general lumpiness of the matrix). On an icy body with a subsurface liquid layer, there may be many ways to create slushy or hummocky, chaos-matrix-like terrain; so we consider only areas with gross morphological characteristics consistent with an exogenic hole-punching origin. We did not include endogenic domes or uplifts, although these features commonly have hummocky chaos-like material associated with them (Pappalardo and Barr 2004). For similar reasons, we excluded features with aspect ratios greater than 4:1. For size-frequency analysis, we measured only chaos areas with boundaries fully imaged by Galileo: thus we did not include the very large chaos regions (≈500–1500 km in longitudinal extent) that cover broad swaths of Europa's surface (Doggett et al. 2007). In addition, detailed mapping in high-resolution images shows that there is much older chaos terrain, heavily overprinted by younger ridges (Riley et al. 2006); but only the young, evident chaos areas were included in this study.

IMPACT PENETRATION ON EUROPA: THE THEORETICAL BASIS

Consensus is growing that thickness, composition, and mechanical properties of the Europan crust vary both laterally and through time (Billings and Kattenhorn 2005; Nimmo et al. 2005). Modest changes in the internal heat flux could cause substantial changes in crust thickness (Mitri and Showman 2005); and differences in grain size, temperature profile, and composition could drive dramatic changes in rheology (Nimmo 2004) such that the ability of the crust to sustain topographic and thickness differences would also vary. Elastic-layer thickness measured at Tyre is about 3–4 km (Kadel et al. 2000), compared with 0.5–2.0 km at Ridge C2 and Androgeos Linea, and 0.2–1 km at Ridge R (Billings and Kattenhorn 2005). Ice thickness beneath Europa's complex craters must have been at least equivalent to the transient crater diameter to prevent the bolides penetrating fully to liquid (Turtle and Ivanov 2002; Turtle 2004). Depth to liquid (total crust thickness) was at minimum 19 km beneath Tyre and Callanish (Schenk 2002), 15 +20/−9 km for the area near Cilix (Nimmo et al. 2003), and but may have been as little as 0.2–3 km at Conamara (Williams and Greeley 1998), and 0.25–3.5 km at Ridge R (Tufts 1998). Hence crust thickness on Europa, at least at some places and at some times, has probably been thin enough for impact penetration to occur.

What bolides can penetrate the Europan ice crust, and how often would such impactors arrive? Numerical simulations suggest that a 1 km diameter comet, impacting at average velocity (26.5 km/s: Zahnle et al. 1998) would cause melt-through of ice 4 km thick, and complete vaporization of ice to 2 km depth (Turtle and Pierazzo 2001). Larger or faster bolides would penetrate thicker ice. The Tyre- and Callanish-producing impactors, estimated to be ≈2 km in diameter (from criteria in Zahnle et al. 2003), caused incipient penetration of the ≈20 km ice crust (Moore et al. 1998; Kadel et al. 2000; Moore et al. 2001; Schenk et al. 2004). If a 2 km bolide fractures crust ≈20 km thick, one 5 km or larger (a 70 km crater-producing event: Zahnle et al. 2003) should demolish it. And such impacts are not rare events: 1 km bolides are expected to arrive at Europa with 2.2 Myr frequency, and the strike rate at Europa for 5 km diameter comets is about 1 per 30 Myr. (Zahnle et al. 2003). Smaller bolides, much more common, would penetrate thinner ice: a 500 m comet, for example, is capable of vaporizing ice to 1 km depth, and completely melting to 2 km (Turtle and Pierazzo 2001). So, if the ice thickness estimations discussed above are reasonable, it's hard to avoid the conclusion that Europa must have been penetrated by impact numerous times. As the strike rate of >2 km bolides is measured in Myr and 10s of Myr (Zahnle et al. 2003), we can expect to find the scars of large impact penetrations even on Europa's young surface.

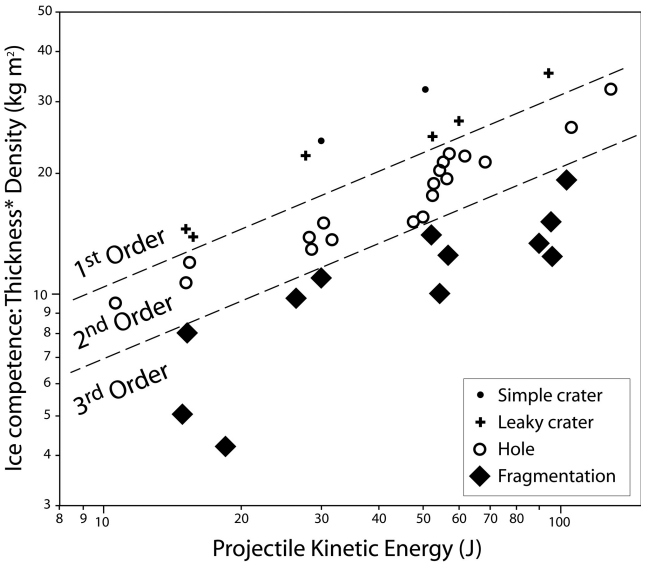

Fig. 2. Results of impact experiments shown as a function of ice competence and impact kinetic energy. The ability of the ice to withstand impact is controlled largely by thickness; but air bubbles within the ice can act as crack nucleation sites (Lange and Ahrens 1981), and so tend to weaken the plate. We used ice-plate density as a measure of the amount of trapped air, and overall plate competence was therefore represented by thickness × density. Dashed lines indicate that boundaries between fields are transitional.

IMPACT EXPERIMENTS

We used the single-stage vertical gas gun at the Institute of Low Temperature Science at Hokkaido University in Japan to make impacts into ice plates over a soft or liquid substrate. The experiments were performed at −15 °C, using cylindrical ice projectiles (15 × 10 mm). The gun setup and methods are described in Arakawa et al. (1995, 2002) and detailed experiment procedures are given in Ong (2004). Impact angle was normal to the surface. Although oblique impacts are the planetary norm, and we know that impact angle can affect the fate of the target (Pierazzo and Melosh 2000), Grey et al. (2002) showed that in ice, crater morphology—especially crater shape—is largely unaffected by impact angles in the range 30–90° to the surface. Impact velocities ranged from 117 to 405 m/s. Our target types were 1) free-floating ice plates resting on water; 2) bonded ice (i.e., frozen to the container edges), with water beneath; and 3) ice plates resting on snow or slush. Ice thickness ranged from 0.5–3.8 cm, and the total depth of each target (ice plus sublayer) was 10–14 cm (Ong 2004).

The free-floating ice plates were made from snow and water. Using snow promoted uniform crystal size in the ice plate, and inhibited crack formation during freezing. The snow was collected from Hokkaido University grounds following fresh snowfall, stored at −15 °C for several months prior to the experiment, then sifted through a 2 mm sieve to remove large crystals. The plates were made by sprinkling 0 °C water onto layers of snow crystals in a 26.5 cm diameter pan. The snow and water mixture was packed down by hand, and the mixture was allowed to sit at −15 °C for two minutes before more snow was added. Layers of snow and water were built up thus until the plate reached the desired thickness, and then allowed to freeze at −15 °C for a minimum of two hours before the ice plate was removed from the pan. Topographic irregularities formed by ice expansion around the edges of the plate were removed with a blade, and the plate was weighed and measured. The plate was finally placed in a 30 cm diameter experiment container, centered on top of the prepared sub-layer. We used three sub-layer materials: snow, slush and water. For *snow sub-layers*, the target container was filled to a depth of 10 cm with loosely-sifted snow crystals <2 mm diameter. *Slush sub-layers* were made using commercially-produced ice spheres of 3 mm diameter placed 3 cm deep in the target container, then covered with water at 0 °C to a depth of 10 cm. For *water sub-layers*, the target container was filled to 10 cm depth with liquid water at 0 °C.

To create stronger, bonded ice layers with no free edges we filled a target container with water to 10 cm depth and let the ice layer form in place. Differing ice thicknesses were produced by varying the freezing time (~6 to 12 h) and temperature (−15 to −7 °C). The ice thus formed made a solid carapace enclosing a liquid water interior.

Ice competence is the ability of the plate to withstand impact. Thickness is the primary control, but not the only one: air pockets or small bubbles within the ice can act as crack nucleation sites (Lange and Ahrens 1981), and so tend to weaken the plate. We used ice-plate density as a measure of the amount of trapped air: denser plates contain less air spaces. Overall plate competence was therefore represented by T × ρ(ice thickness × ice density) (Fig. 2). We estimated density in two ways. The free-floating snow-and-water ice plates could be handled independently of the experiment container, so we measured thickness, diameter, and weight directly. The calculated densities ranged from 0.72–0.99 g/cm^3 (Table 2). These plates were milky in appearance because air was trapped among the snow crystals, so the low density values were expected. The upper value, however, is clearly an overestimate, which we attribute to imprecision in the thickness measurements caused by small-scale roughness on the ice plate surfaces. Thickness measurements are accurate to ±1 mm, and we calculate a consequent maximum error in the density estimates of is about 0.07 g/cm^3 (given by the difference between the maximum calculated density and the known density of ice Ih at −15 °C). The remaining 0.2 g/cm^3 (30%) variation in calculated plate densities therefore represents real differences in amounts of trapped air and hence plate competence. For bonded-ice targets we could not weigh the ice prior to the experiment because it was stuck to the experiment container, so we used the standard density of 0.92 g/cm^3 for ice between −7 and −15 °C (Lide 2002). This was justified by extreme clarity of the bonded ice targets, indicating that they contained few or no air bubbles.

The result in each experiment (Table 1) was governed by

Table 1. Results of impact experiments carried out at −15°C, with cylindrical ice projectiles (15 × 10 mm, and mass 1.6 g). Further details on methods in text.

Shot	Impact type		Substrate	[a]Ice type	[b]Ice plate thickness (cm)	Ice plate diameter (cm)	[c]Ice plate mass (kg)	[d]Target density (kg/m^3)	[e]Plate competence (kg/m^2)	Projectile velocity (m/s)	[f]Projectile mass (g)	Projectile density (kg/m^3)	Impact energy (J)	[g]Impact Intensity	[h]Impact site diameter (cm)	First-order crater depth (cm)	[i]Transient hole diam. (cm)	No. of fragments (>1 cm)
T030	First order	Simple crater	Water	F	2.4	26.5	1.24	980	24	190	1.60	905	29	1.2	3	0.32		
T039	First order	Simple crater	Water	F	3.5	26.5	1.76	910	32	252	1.59	900	50	1.6	4.1	0.43		
T007	First order	Leaky crater	Snow	F	1.4	26.5	0.78	990	14	140	1.57	888	15	1.1	3.4	1.00		
T013	First order	Leaky crater	Water	F	1.6	26.5	0.76	890	14	140	1.57	888	15	1.1	2.0	0.37		
T037	First order	Leaky crater	Water	B	2.4	30.0	–	920	22	184	1.59	900	27	1.2	2.6	2.10		
T033	First order	Leaky crater	Water	F	3.0	26.5	1.32	810	24	261	1.58	894	54	2.2	5.1	0.60		
T034	First order	Leaky crater	Water	F	3.2	26.5	1.28	740	24	278	1.58	894	61	2.6	3	3.15		
T041	First order	Leaky crater	Water	F	3.8	26.5	1.90	910	35	352	1.57	888	97	2.8	5.4	0.60		
T005	Second order	Hole	Snow	F	1.0	26.5	0.53	950	10	117	1.55	877	11	1.1	2.7			
T011	Second order	Hole	Slush	F	1.2	26.5	0.60	890	11	139	1.57	888	15	1.4	3.6			
T031	Second order	Hole	Water	B	1.3	33.5	–	920	12	140	1.58	894	15	1.3	2.6			
T028	Second order	Hole	Water	F	1.5	26.5	0.74	920	14	189	1.58	894	28	2.0	2.7			
T032	Second order	Hole	Water	B	1.4	42.0	–	920	13	190	1.58	894	29	2.2	2.4			
T042	Second order	Hole	Water	B	1.4	33.5	–	920	13	191	1.58	894	29	2.2	4.0			
T026	Second order	Hole	Water	F	2.0	26.5	0.85	750	15	195	1.60	905	30	2.0	2.8			
T014	Second order	Hole	Water	F	1.5	26.5	0.75	910	14	201	1.57	888	32	2.3	3.2			
T016	Second order	Hole	Water	F	1.8	26.5	0.82	840	15	246	1.58	894	48	3.2	5.2			
T027	Second order	Hole	Water	F	1.6	26.5	0.85	970	16	252	1.58	894	50	3.2	3.6			
T020	Second order	Hole	Water	B	1.9	47.0	–	920	17	259	1.57	888	53	3.0	3.9			
T038	Second order	Hole	Water	F	2.1	26.5	1.01	890	19	258	1.59	900	53	2.8	4.1			
T036	Second order	Hole	Water	B	2.2	33.5	–	920	20	263	1.57	888	54	2.7	3.6			
T025	Second order	Hole	Water	F	2.5	26.5	1.15	850	21	263	1.60	905	55	2.6	3.2			
T021	Second order	Hole	Water	B	2.1	30.0	–	920	19	268	1.57	888	56	2.9	2			
T002	Second order	Hole	Snow	F	2.5	26.5	1.23	890	22	269	1.58	894	57	2.6	2.7			
T024	Second order	Hole	Water	B	2.7	30.0	–	920	25	280	1.58	894	62	2.5	3.3			
T022	Second order	Hole	Water	B	2.3	33.5	–	920	21	295	1.57	888	68	3.2	4.8			
T017	Second order	Hole	Water	B	2.8	33.5	–	920	26	366	1.58	894	106	4.1	4.9			
T018	Second order	Hole	Water	B	3.8	30.0	–	920	35	405	1.57	888	129	3.7	6.5			
T001	Third order	Fragmentation	Water	FR	1.6	21 × 17	0.55	920	15	337	1.55	877	88	6.0	–		–	40
T040	Third order	Fragmentation	Water	B	0.5	30.0	–	920	5	152	1.57	888	18	3.9	12		8.0	33
T035	Third order	Fragmentation	Water	B	1.4	30.0	–	800	11	261	1.58	894	54	4.8	23		3.5	14
T029	Third order	Fragmentation	Water	B	0.9	30.0	–	920	8	140	1.57	888	15	1.9	7		–	10
T023	Third order	Fragmentation	Water	B	2.1	47.0	–	920	19	363	1.58	894	104	5.4	8.2		6.0	16
T019	Third order	Fragmentation	Water	B	1.9	33.5	–	920	17	350	1.54	871	94	5.4	12		–	16
T012	Third order	Fragmentation	Slush	F	1.4	26.5	0.75	970	14	349	1.56	883	95	7.0	26		8.0	20
T009	Third order	Fragmentation	Slush	F	1.3	26.5	0.65	880	11	196	1.57	888	30	2.6	8.6		2.7	5
T008	Third order	Fragmentation	Slush	F	1.5	26.5	0.79	960	14	256	1.60	905	52	3.6	7		3.9	11
T006	Third order	Fragmentation	Snow	F	0.7	26.5	0.29	720	5	138	1.56	883	15	2.9	2.8		2.3	6
T004	Third order	Fragmentation	Snow	F	1.1	26.5	0.54	890	10	183	1.58	894	26	2.7	3.2		2.8	8
T003	Third order	Fragmentation	Snow	F	1.4	26.5	0.69	900	13	267	1.60	905	57	4.5	6		2.4	9

[a]F = Free-floating circular ice plate; B = bonded circular ice (i.e., ice frozen to container walls); FR = Free-floating ice rectangle.
[b]Ice plate thickness measurements at plate centre are ± ≈1mm. For *free-floating* plates, this is representative of the entire plate. For *bonded plates* it is a minimum value because plates thickened toward the pan walls.
[c]Ice plate mass measured pre-experiment for free-floating plates; this measurement was not possible for bonded targets that, once formed, were inseparable from the target container.
[d]Target density calculated for free-floating plates; standard density used for bonded plates. See Methods for details.
[e]Plate competence is the product of thickness times density. See text for details.
[f]Ice projectiles were cylinders 1 cm high and 1.4 cm diameter.
[g]Impact intensity is the ratio of impact energy and plate competence. See text for details.
[h]Diameter of crater, hole, or total destroyed zone for first-, second-, and third-order impacts.
[i]For third-order impacts: the diameter of the initial bolide puncture, measured post-experiment by reconstructing the scattered fragments. n.d. indicates that the degree of fragmentation did not permit reconstruction of the transient hole.

Table 2. Small-crater (50–870 m diameter) counts from high-resolution Galileo observations E17THRACE01, E17LIBLIN01, and E17AGENOR03B. Craters were mapped at a scale of 1:70,000, using a Mercator projection in ArcMap. Images were reprojected into a sinusoidal data frame to calculate the areas. Numbered subdivisions represent the portion of each image contained within a specific half-radius (20 km) distance of Thera centre (see Fig. 7). Total crater N = 1478.

	E17THRACE01			E17LIBLIN01			E17AGENOR03b			Total Mapped		
Thera radii from center	Area[a] (km^2)	No. of craters		Area (km^2)	No. of craters		Area (km^2)	No. of craters		Total craters	Total area (km^2)	Crater (s/km^2)
3.0–3.5	**T1**	175	56							56	175	0.31
3.5–4.0	**T2**	751	84	**L1**	491	222				306	1242	0.20
4.0–4.5	**T3**	823	114	**L2**	1103	390				504	1926	0.23
4.5–5.0	**T4**	294	27	**L3**	601	203	**A1**	684	84	314	1579	0.15
5.0–5.5	**T5**	295	41				**A2**	1140	75	116	1435	0.05
5.5–6.0	**T6**	492	37				**A3**	896	32	69	1388	0.04
6.0–6.5	**T7**	18	1				**A4**	1169	52	53	1187	0.04
6.5–7.0							**A5**	807	58	58	807	0.06
7.0–7.5							**A6**	89	2	2	89	0.02

[a]In the E17THRACE01 observation, about 1200 km^2 of the imaged ground is occupied by knobby material of Thrace Macula (Fig. 7), in which small craters are not seen; so we did not include that portion in the crater-counted area.

the interplay between impact energy and ice competence. We divided the outcomes into first- through third-order events, classifying them on the basis of significant shifts in the type of damage done by the impactor (Fig. 2).

First-Order Events Produce Craters: Both Simple and Leaky

At lowest impact intensity (low impact energy or thick ice), standard craters formed, such as those produced in solid-target experiments (e.g., Kato et al. 1995; Arakawa 1999), with damage confined to the upper part of the ice plate and no involvement of the sublayer. We induced incipient penetration by raising impact intensity (by increasing impact energy or decreasing ice thickness) to the point where impact damage extended through the full thickness of the ice. Incipient penetration resulted in leaky craters, in which through-going cracks penetrating to the fluid sublayer allowed upward bleeding of liquid (Figs. 3a and 3b) that partially filled the impact site. The leaked material was confined to the bowl-shaped impact site. Different substrates did not appear to affect the impact outcome in terms of penetration versus non-penetration: there was no systematic difference among the snow, slush, and water experiments.

Second-Order Events Produce Holes with Simple Shapes and Few or No Rafts

At higher impact intensity (thinner ice or higher impact energy), projectiles penetrated fully. The lowest-intensity penetrations were equidimensional openings (circular or angular) punched cleanly through the ice (Figs. 3c and 3d). They contained a slushy mixture of pulverized ice and exposed fluid, with few or no large ice fragments. Hole walls were steep to vertical in the upper cm of the plate, but flared away from the impact site in the sub-surface to give an hourglass-shaped cross section (Fig. 5), matching that produced in hydrocode simulations of penetrating impacts (Ivanov and Turtle 2001; Turtle 2004). Overall, second-order holes represented clean perforations through the ice, looking like bullet holes. The size of the holes is a function of impact energy, and scales with crater size both in these experiments (Table 2, Fig. 4a) and in comparison with published solid-target ice-impact data (Ong 2004).

Third-Order Events Produce Fragmentation Zones with Lots of Rafts

At highest impact intensity (greatest impact energy and/or thinnest ice), there was a dramatic change in impact dynamics, with the projectile not only penetrating but also causing wide-field fragmentation of the ice plate. These third-order impacts destroyed the ice layer at a considerable distance from the impact site, generally leaving a jagged and irregular hole. The asymmetrical destroyed zone was filled with slushy liquid, finely pulverized ice, and large ice rafts (Figs. 3e and 3f). Rafted fragments were rotated, translated, and sometimes tilted by turbulence within the fluid. Tilt angles ranged from a few degrees to fully vertical, and in some cases blocks were thrust over one another. Post-experiment reconstruction of the pieces revealed that the initial impact produced a transient hole, resembling a second-order bullet hole, which was significantly smaller than the final destroyed zone. This suggests that the initial penetration was clean, like a second-order impact; but the higher relative energy caused subsequent disintegration of the surrounding plate.

Fragmentation was probably due to a combination of shock wave propagation through the ice layer, and ice-layer flexure induced by gravity waves at the ice-water interface

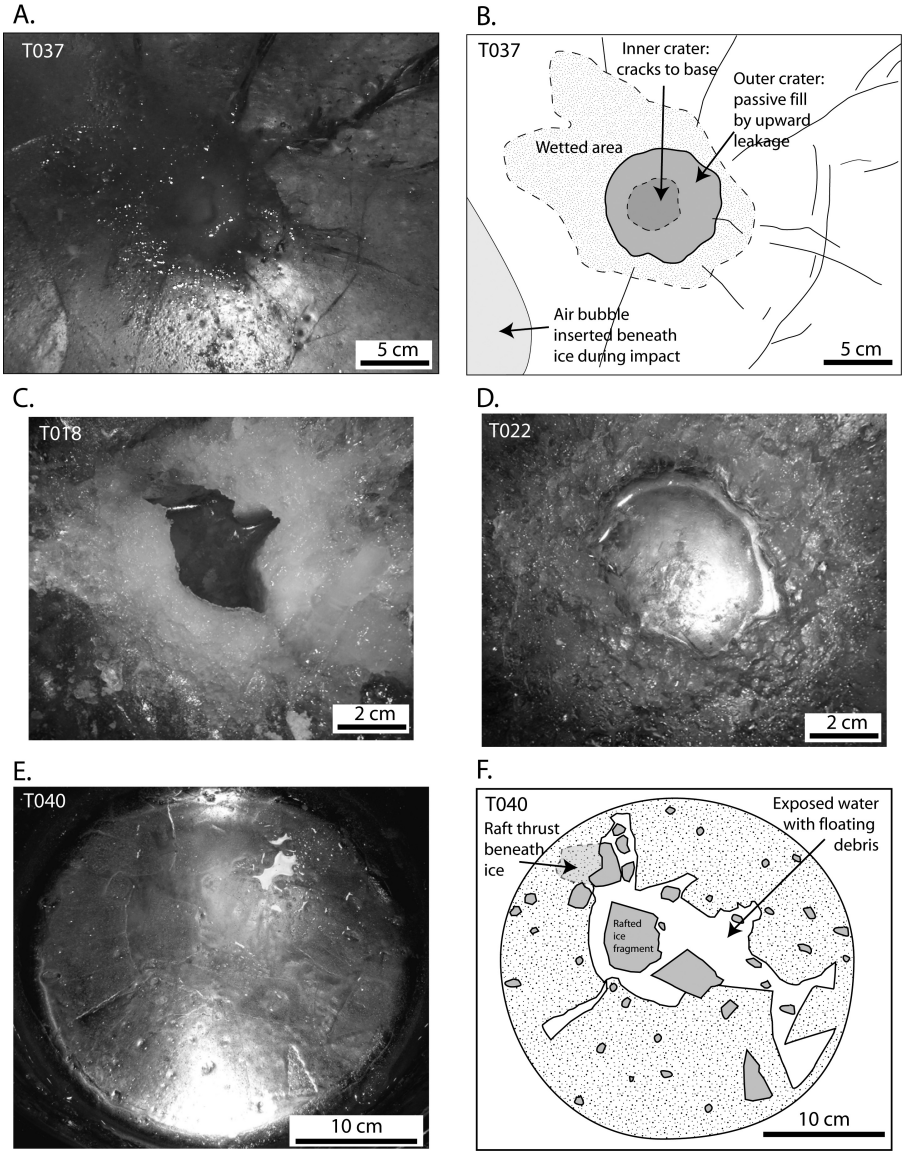

Fig. 3. Examples of experiment outcomes. a and b) Photograph and line drawing of first-order leaky crater (incipient penetration). c) Photograph of second-order impact (angular hole). d) Photograph of second-order impact (circular hole). e and f) photograph and line drawing of third-order impact (wide-field fragmentation), showing the irregular shape of the destroyed area, abundant ejecta, and chaotic redistribution of ice fragments.

(Billings and Kattenhorn 2003). Because of this post-impact hole-widening effect, the destroyed zones were generally larger than holes or craters formed at similar impact energies (Fig. 4a). The rafts that characterized these third-order events were by-products of the fragmentation process by which the destroyed zone expanded. The degree of destruction increased with impact intensity: more energetic impacts, or impacts into thinner ice, produced bigger destroyed zones (Fig. 4a) with more numerous and relatively smaller rafts (Fig. 4).

Impacts into ice over snow produced smaller holes than similar impacts into ice over water or slush (Fig. 4a), and there was also a tendency, albeit less marked, for less raft production in snow-subsurface experiments (Fig. 4b). We interpret this as due to the stiffness of the snow relative to slush or water, and suggest that it illustrates the importance of gravity waves on the water surface in producing relative motions that contribute to opening cracks in the ice, and translating the freed blocks.

LABORATORY IMPACT MORPHOLOGIES COMPARED WITH EUROPAN CRATERS AND CHAOS AREAS

Impact outcome depends on the relationship between bolide energy and crust competence, so small bolides in thin crust or large bolides in thick crust might produce similar geomorphologies. In addition, temperature may play a role in

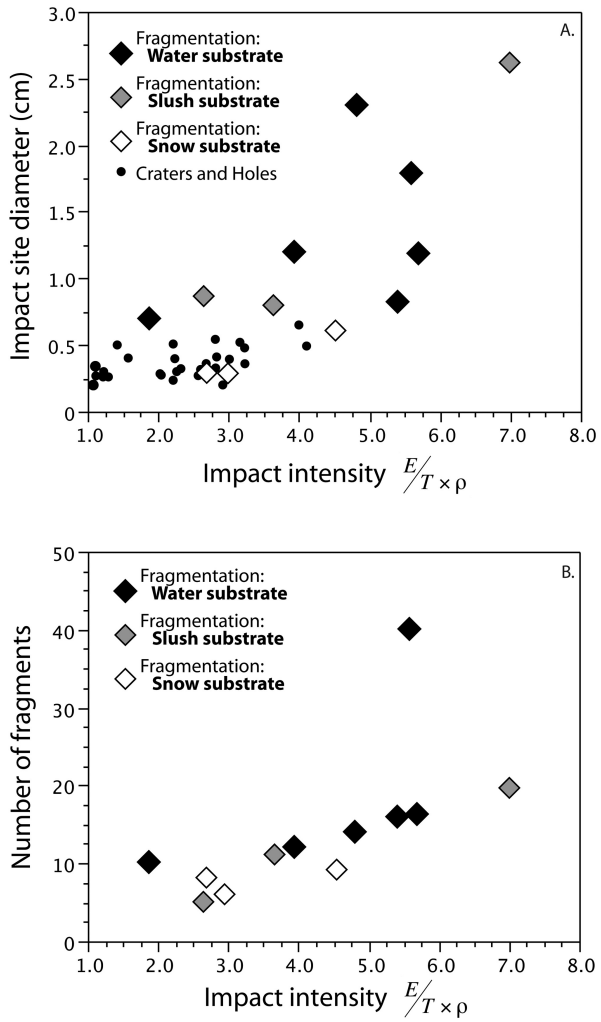

Fig. 4. a) Impact site diameter as a function of impact energy. The size plotted is the final crater or hole diameter. For any given energy, first-order impacts (craters) and second-order impacts (holes) will have smaller diameters than third-order fragmentation events. Transient hole sizes—measured by reconstructing the fragment jigsaw after the experiment—are not shown on this diagram, but are generally of the same order as the first- and second-order equivalent-bolide features (see Table 1). The post-impact fragmentation processes in third-order impacts dramatically expand the size of the hole. b) Large fragments (>1cm width) in third-order impacts as a function of impact intensity. Impact intensity is the ratio of E (impact energy) to ice competence ($T \times \rho$). Impacts at higher energy, or into less competent ice, generate larger numbers of fragments, most of which remain in the impact site.

the geometry of impact features in ice (Grey and Burchell 2003), although this is not yet quantified at planetary scales. Our schematic diagrams (Figs. 5a–c) are cartoons therefore, with no implied characteristic size. Updoming of the matrix can be caused by ice thickening during freezing, assuming that the newly forming ice welds to the walls of the chaos area, as seems probable (Nimmo and Giese 2005). Relative uplift of matrix, and cliffed versus onlapping boundaries, will depend on the buoyancy and freezing rate of the exposed fluid, as well as on subsurface pressure gradients.

First-Order Impacts: Craters and Leaky Craters

First-order craters are well described from Europa (e.g., Bierhaus et al. 2001b; Moore et al. 2001), but none are very big. The 2×10^5 tiny craters (<1 km diameter) mapped on 0.2% of Europa's surface suggest about 8.5×10^6 in total (Bierhaus et al. 2005), but there are only 24 known first-order impacts ≥10 km (Schenk et al. 2004). Although incomplete coverage of Europa's surface implies that more medium-sized impacts remain to be discovered, we can say with confidence that all first-order impacts are less than 50 km in diameter. Maeve (20 km) is the largest undisputed solid-target impact. The two biggest features, Callanish (≈33 km) and Tyre (≈40 km), are both incipient-penetration structures, considered to record impact cracking of the crust and seepage of fluid from below (Moore et al. 1998; Kadel et al. 2000; Moore et al. 2001; Greenberg and Geissler 2002).

There may be a spectrum of impact scars, from pure solid-target to borderline penetration. For example, craters such as Amergin (19 km), Manannán (22 km), and Pwyll (24 km) have chaos-like basin fill, possibly representing leaked and refrozen subsurface fluid (Greenberg 2005; Greenberg and Geissler 2002). If so, then they may represent the "slightly leaky" transition from true solid-target to incipient penetration structure. Tegid and Taliesin (≈28 km), although both poorly imaged (1.44 and 0.75 m/pixel, respectively), share similarities with Tyre and Callanish, suggesting that they are transitional to multi-ring features (Moore et al. 2001), thus possibly representing incipient penetration by smaller bolides in thinner crust.

Leaky craters form for a restricted subset of bolide size and crust thickness, and therefore are not expected to be numerous. Tyre and Callanish are good candidates, and Tegid and Taliesin may be additional examples. But why do we do not see smaller versions of Callanish and Tyre in areas where ice may be thin enough for smaller bolides to penetrate and form chaos? The answer may relate to the difficulty of imaging the subtleties of such features at the available scales. Tegid, with its 28 km diameter inner rim and ≈80 km total diameter, imaged at 1.44 km/pixel, is ≈55 pixels across, and yet difficult to classify because the annular structure is fuzzy and ambiguous (Moore et al. 2001). A 13 km feature in 250 m/pixel regional imagery would likewise be about 55 pixels across, and as the scale of the rings would be similar to the scale of background ridged terrain, the resulting feature would be unclear at the resolution of most Galileo imagery.

Second-Order Impacts: Holes

Chaos areas with hummocky or blocky matrix, but few or no large rafts ("knobby chaos" of Greeley et al. 2000), resemble second-order impact holes. The "Mitten," Murias Chaos (Greenberg et al. 1999; Figueredo et al. 2002), might fall in this category. Murias Chaos has a broadly circular outline (excluding the "thumb"), and sharp boundary scarps

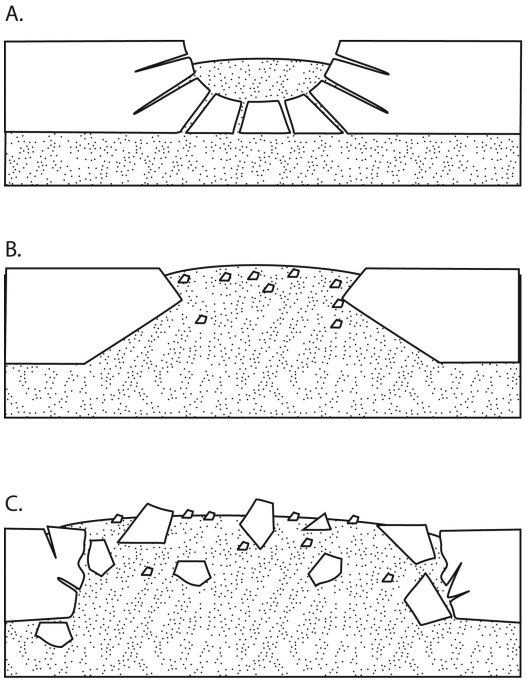

Fig. 5. Schematic diagram of impact outcomes at constant crustal thickness with increasing impactor energy. Elevation of matrix is near or greater than the surrounding topography, and is governed by vertical pressure gradients (which may force the sublayer material up) and also by the viscosity and salinity of the sublayer material, which will affect the freezing rate. a) First-order impact, leaky crater, with cracks penetrating to fluid in subsurface. b) Second-order impact hole. The impact site has an hour-glass shaped cross section, and is filled by a slushy mixture of pulverized crust and impactor plus sub-layer material, producing the characteristic hummocky chaos texture. Although as yet unconstrained by modelling or experiment, it is possible that the impact hole corresponds in size approximately to the transient crater diameter of a solid-target impact. c) Third-order impact causes widespread fragmentation of a large area of the crust. The destruction area is substantially greater than the transient hole of the impact site. The fill is a slushy matrix of pulverized crust and impactor plus sub-layer material, containing large blocks of displaced crust from the wider destruction area. The right-hand side of C shows a steep escarpment as the chaos boundary, where matrix is lower than the elevation of the fractured crust. The left-hand contact is extrusive, with sublayer material onlapping the older surface.

with down-to-the-center displacement (Fig. 1c). The matrix is updomed, although whether it is elevated above the bounding scarps is debated (Figueredo and Greeley 2000; Riley et al. 2000; Figueredo et al. 2002). The "thumb" shows onlap contact with the surrounding terrain, suggesting matrix overflow (Riley et al. 2000); and the boundary fractures at the southern edge appear to have been mantled by extruded matrix material. Resurgence of the matrix has onlapped the surrounding surface around most of the perimeter, and in the southeastern quadrant it has caused crustal blocks to tilt outward. There are knobs and blocks embedded in the matrix, but with few exceptions their sizes are small relative to the diameter of the chaos area. Murias is unusual in being a large chaos area dominated by knobby, raftless chaos terrain. Most examples of second-order chaos on Europa are only a few km in diameter (Figs. 1a and 1b), but all share the characteristics of being approximately equidimensional, and dominated by matrix. These may represent sites where impactors punched cleanly through the ice crust, without causing wide-field fragmentation of the surrounding area.

Third-Order Breaches: Jagged Holes with Rafts

In contrast to the regularly-shaped second-order knobby chaos features, platy chaos areas (sensu Greeley et al. 2000) characteristically have irregular outlines, sharp scarp-like edges, and abundant rafted blocks, like the third-order wide-field-fragmentation impacts in our experiments. Although there are resolution issues with distinguishing between platy and knobby chaos at small sizes, the average size of platy chaos appears to be greater than that of knobby chaos, and they range from several km to more than 100 km in diameter (e.g., Figs. 1d–g). Most of the large chaos areas on Europa (Murias Chaos being a rare exception) are raft-dominated third-order features. Thera Macula (Fig. 1g) is a particularly spectacular example. It has a very irregular outline, and numerous large rafted and tilted crustal blocks, including some that have not fully detached from the edge. These are candidates for impact sites where shock wave and/or gravity wave propagation exceeded the strength of the brittle crust at distances beyond the transient crater diameter, causing widespread fragmentation and raft formation.

Some third-order-type chaos areas are bounded by and appear to be kerbed by pre-existing ridges, indicating that the ridges are resistant to the chaos-forming processes (Greenberg et al. 1999). Figure 1d is a good example of this phenomenon. Greenberg et al. (1999) have also pointed out that some chaos initiate "squarely on the site of ridges" (e.g., Fig. 1c), and that these two observations form important constraints on models of chaos formation. In the context of our hypothesis, chaos forming on a ridge site simply means that the impactor hit there. The case of chaos areas bordered by ridges implies that the ridges are stronger—because thicker—than the intervening plains, and therefore limit post-impact fracture propagation. The effect of pre-existing tectonic fabric on non-penetrating impacts has also been noted: craters Amergin and Maeve have polygonal outlines interpreted to be controlled by older ridges (Figueredo and Greeley 2004).

Conamara Chaos (Fig. 6) is unusual in having a very high proportion (≈40% by area) of large blocks (Spaun et al. 1998): most large chaos areas have a much greater preponderance of matrix (see Fig. 1). The question is, can an impactor be fit into this, or is an impact origin impossible with such a dense concentration of large rafts? Two relationships suggested by our experiments indicate that Conamara could represent an impact site. First, large numbers of blocks are generated by high-intensity impacts (Fig. 4a); and for a given impactor energy, higher-intensity impacts occur in thinner ice (Fig. 2). Conamara Chaos is 110 km ECD, but measurements from

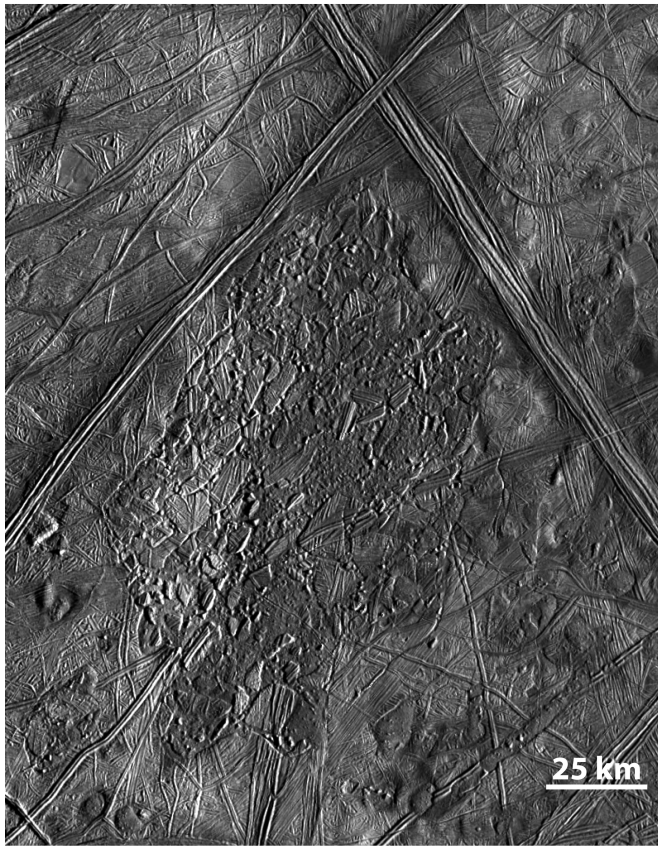

Fig. 6. Composite of Galileo images of Conamara chaos. Conamara is 40% blocks and 60% matrix by area (Spaun et al. 1998).

tilted ice rafts indicate elastic layer thickness of only 0.1–0.5 km, and total thickness of <3 km (Williams and Greeley 1998). Second, the destroyed zone of an ice-penetrating impact can be much larger than the non-penetrating equivalent: for example, third-order impacts generated destroyed areas with diameters more than 4 times greater than first-order craters formed at equivalent impact energy (Fig. 4b). The largest destroyed zone in our experiments had diameter 15 times that of the projectile and 7 times that of the transient hole (Table 1). One of the factors contributing to increased diameter was ice thickness: all else being equal, the damage radius is larger in thinner ice. So, although we note that the scaling factors relating destroyed zone size to bolide geometry are not quantified, and that we do not yet know how the mechanisms of fracturing and block formation would work at planetary scales, these results permit the hypothesis that a relatively small bolide could generate the large, raft-dense destroyed zone represented by Conamara Chaos. The central area would have been largely raft-free immediately post-impact, but the cleared area was reduced in size by inward migration and current-driven rotation of rafts (Spaun et al. 1998). The clockwise rotation documented by Spaun et al. (1998) is consistent with seiche motions in the disturbed liquid.

Raft Formation by Impact

Three distinct processes could contribute to raft formation: spallation, shock wave damage, and gravity wave propagation. If the thickness of the spallation layer is close to that of the solid ice, then some rafts may represent spall plates. As the ejection angle from impacts into water is close to vertical (Gault and Sonett 1982), third-order impact ejecta will have steep ballistic trajectories and thus many are likely to fall back into the opening chaos area. Shock wave stress differentials are also likely to result in widespread plate fracture. The stress wave propagates more rapidly in solid ice than in liquid water, and the resulting net shear across the ice-water boundary is predicted to cause disruption at several crater radii from the impact site (Moore et al. 1998). This process would be aided and enhanced by tsunami-like post-impact gravity waves generated in the exposed fluid (Gault and Sonett 1982; Weiss et al. 2006), which would propagate away from the impact site along the ice-water boundary, flexing and cracking the ice layer (Billings and Kattenhorn 2003; Billings 2004). Both wave action (including seiches likely to reverberate around the impact hole) and turbulence in the fluid would contribute to moving and tilting the liberated blocks.

WHAT ABOUT SECONDARY CRATER PRODUCTION?

Analysis of secondary crater fields from different crater types on Europa suggests that when the liquid substrate is felt by the impactor, ejecta formation is suppressed. For example, both Callanish (diameter ≈33 km) and Tyre (≈40 km) have essentially the same secondary-crater density as the much smaller (24 km) Pwyll (Moore et al. 1998; Bierhaus 2004); which may reflect less effective production of solid ejecta by the larger impacts because of liquid sublayer involvement (Moore et al. 1998). This interpretation is consistent with hydrocode modelling, which predicts that underlying liquid affects the physics of incipient-penetration impacts so that they produce fewer ballistic fragments, with lower average velocity (Moore et al. 1998). By extension, fully penetrating impacts would be expected to produce yet fewer and probably slower ejecta. Additionally, the ejection angle for material emanating from liquid is close to 90° (Gault and Sonett 1982), which means that a large proportion of ejecta would fall directly back into the impact hole. This would be especially true for third-order breaches, where the destroyed zone is very large with respect to the impact energy (Fig. 4a). Thus, a relatively small proportion of solid ejecta would have ballistic trajectories taking them beyond the impact site boundaries. High-speed imaging of hypervelocity impacts into ice-over-liquid supports these predictions, showing that ejecta have steep trajectories (60–90°) and low velocities (<1% of impact velocity) (Scheider and Cox 2007).

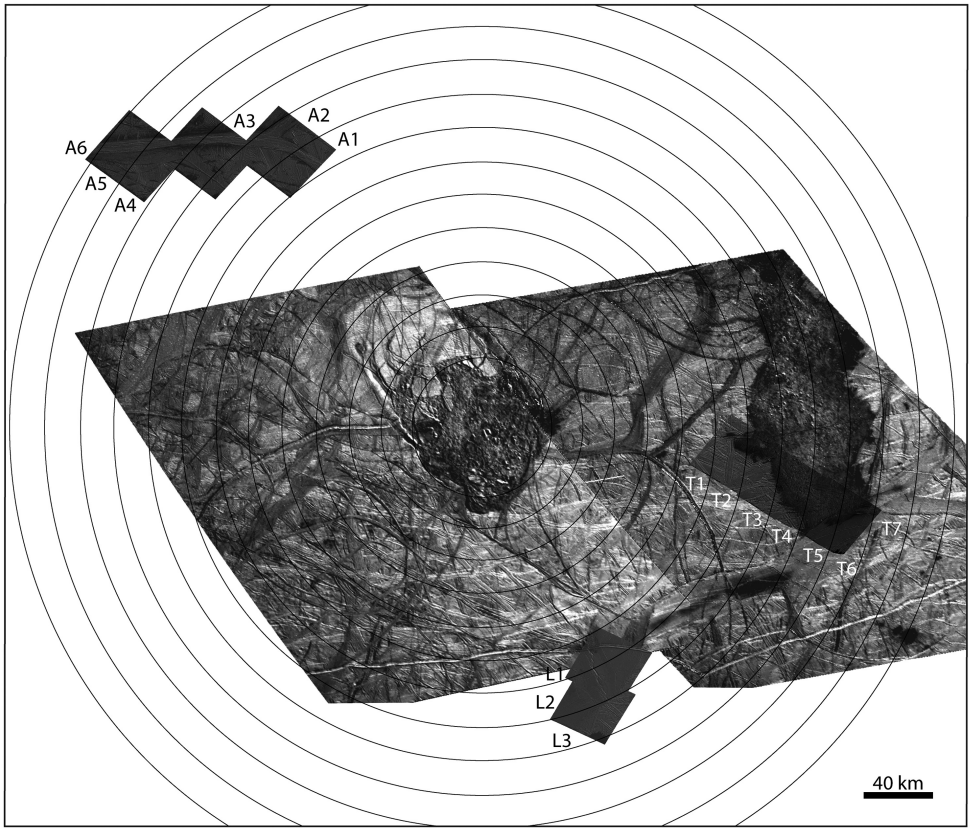

Fig. 7. Galileo image mosaic of the region around Thera and Thrace macula, in sinusoidal projection. The background image resolutions are only 250–360 m/pixel; but the high-resolution inserts (i.e., E17LibLin01: L1-L3, E17Agenor03b: A1–A6, and E15Thrace01: T1–T7: see Table 2) are 40–50 m/pixel, at which craters 200–1000 m diameter can be mapped with confidence. Only craters from the high-resolution images—of which there are 1478—are used in our analysis. Circles are in increments of 1 Thera radius (ECD). Within the high-resolution inserts, the half-radius boundaries are shown but the craters themselves are invisible at this resolution. The letters and associated numbers designate half-radius divisions of the high-resolution observations (see Table 2). Thera's ECD is ≈80 km, so the area enclosed within 7.5 Thera radii is ≈283,000 km^2. Of this, ≈240,000 km^2 is contained in the annulus between 3 and 7.5 radii, i.e., the region where the high-resolution images are located; the images cover 19,000 km^2, or 8% of the annulus. The data are shown in Table 2 and Fig. 8.

These constraints suggest that secondary-crater fields around impact-formed chaos would be much less densely populated than those around comparable solid-target or incipient-penetration impacts, and that the mean and maximum sizes of secondary craters would likewise be smaller. This is difficult to test with Galileo imagery, because excepting Conamara (which lies within the Pwyll ejecta field) no large chaos areas are imaged at better than ≈250 m/pixel. Such resolutions are adequate to reveal the secondary fields around impacts such as Pwyll or Tyre, where about half the secondary craters are >1 km (Bierhaus 2004, 2006); but as reliable feature recognition drops off rapidly below 4 pixels diameter, small-crater populations would not be mappable on these images.

There is, however, one place on Europa where we can demonstrate a chaos-related secondary crater field dominated by very small craters: the region around Thera Macula (≈80 km ECD). Although only a few craters (600–1600 m diameter) are evident in the 250–350 m/pixel regional images (E17 images 4401 and 4413; Fig. 7), there are strong indications in the imagery that numerous additional craters exist below the limits of resolution. Luckily, three high-resolution (41–48 m/pixel) mosaics surround Thera at 125–300 km (3–7.5 Thera radii) from the center of the chaos area (Fig. 7), all of which are liberally peppered with small craters that have been classified as secondary craters based on size and clustering (Bierhaus 2004; Bierhaus et al. 2005), but which have not previously been tied to a primary impact source. We have mapped in these images ≈1500 craters 50–870 m in diameter, with 97% <500 m. The crater densities—in aggregate and from each individual image mosaic—show logarithmic decrease as a function of distance from Thera (Table 2, Fig. 8), suggesting that they emanated from Thera Macula.

A key observation here is the very small number of secondary craters around Thera, in comparison to the secondary fields around impacts such as Tyre and Pwyll. The enormous magnitude of the secondary population within Pwyll's ≈1000 km diameter ray system is well documented (Bierhaus et al. 2001b): there are an estimated 10^6 secondary craters in the rays alone, not counting the well-peppered inter-

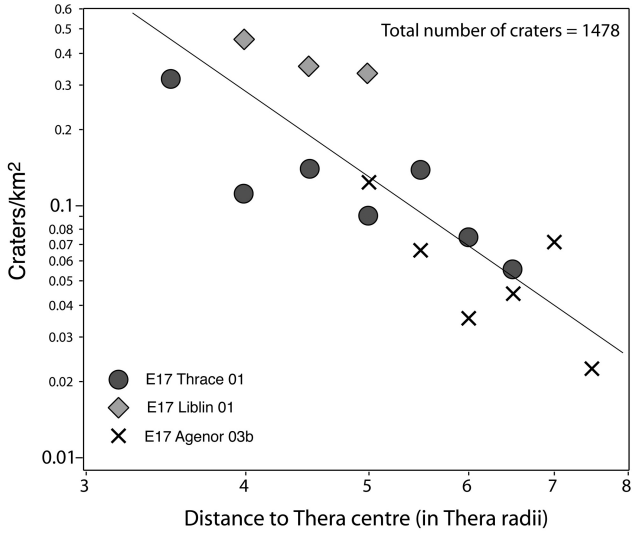

Fig. 8. Density of small craters (diameter 0.2–1.0 km, mapped from the Thrace, Agenor, and Libya high-resolution mosaics shown on Fig. 7) as a function of distance from the center of Thera Macula. The data show a steep logarithmic decline in numbers of small craters away from Thera, consistent with decay of a secondary crater population with distance from the primary source. The solid black line is the best fit through the combined data set (all craters as a function of distance from Thera, not separated by mosaic as shown here) and has the form $\log(y) = 3.3–3.4 \log(x)$, with $R^2 = 0.86$. The data represent 100% of the resolvable craters from the 8% of the area between 3 and 7.5 Thera radii that is imaged by the high-resolution observations.

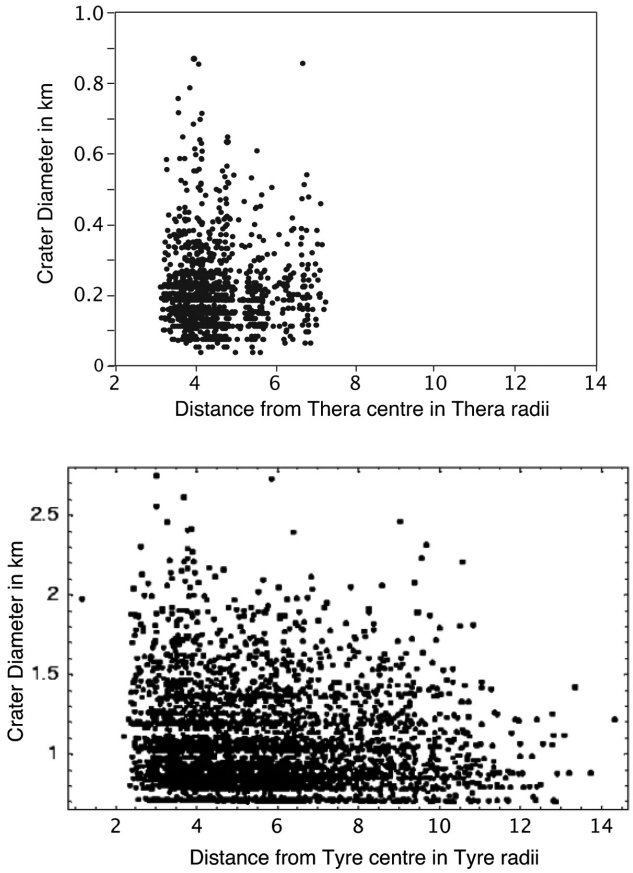

Fig. 9. The upper graph shows the size-distance relationships for small craters mapped in the high-resolution (<50 m/pixel) images around Thera. The lower (from Bierhaus [2006]) shows data from the ≈200 m/pixel E14TYRE01 mosaic. The measurements appear quantized at smaller diameters because of pixilation. The X axes are to the same relative scale, but note the very different scale on the Y axes. Although Thera is a factor of two larger than Tyre, the secondary craters around Thera are much smaller on average. Both data sets show largest craters closest in, and a drop-off in both size and numbers of craters with greater distance. For the Thera data, there is no correlation between the amount of area mapped and the abundance of larger craters: the most proximal regions have small mapped image areas (Table 2), yet have the largest craters.

ray area (Bierhaus, personal communication). In contrast, the number of confidently identified craters in the 9700 km^2 of high-resolution imagery surrounding Thera is 1.5×10^3 (Table 2). Extrapolating to the 207,300 km^2 of terrain lying between 3 and 7 Thera radii, we predict 3×10^4 secondary craters, and only about 6×10^4 at 14 Thera radii. By comparison, Tyre created 7×10^3 craters >1 km—and probably 10^5 secondary craters total—within 14 Tyre radii, the vast majority being within 7 Tyre radii (Bierhaus 2006; and Bierhaus, personal communication). A direct comparison between the near-field areas of Thera and Tyre indicates that Thera's secondary crater population is at least a factor of two smaller than that around Tyre.

The secondary craters surrounding Thera are not only few but small. The largest crater in the high-resolution images is 0.9 km, and the largest in the regional images (Fig. 7) is 1.6 km diameter. The largest crater in the Tyre secondary field, in contrast, is 2.7 km (Bierhaus 2006), and the field includes at least 50 craters >2 km (calculated from data in Bierhaus 2004). Likewise—although Thera is twice the size of Tyre—the average diameter in the Thera secondary field is only 400 m, less than half the 1000 m median size for Tyre secondary craters. The maximum crater size also decreases with distance, and the size-distance distribution shows a remarkably similar pattern—although much smaller in scale—to that of the Tyre secondary field (Fig. 9). Similarly, the secondary crater densities at 3–5 Thera radii (Table 2) are comparable to those at 100 Pwyll radii: data from 50 m/pixel images in both cases give averages of 0.03 craters/km^2 (Pwyll data from Bierhaus et al. [2001b]).

Our observations of few and small secondary craters around Thera are in accord with the prediction, based on comparisons between Callanish and Pwyll, that impacts into ice over water produce fewer and slower ejecta than impacts into solid ice (Moore et al. 1998). The radically different secondary crater numbers, sizes, and densities suggest that second and third order impacts produce very meagre secondary crater populations, orders of magnitude less numerous than non-penetrating impacts (like Pwyll) or incipient-penetration impacts (such as Tyre).

Europa's Secondary-Crater Populations: Arguments That They May Not All Be Produced by the Known Primary Impacts

The majority of Europa's small craters (diameters <1 km) are probably secondary in origin (Bierhaus et al. 2001a, 2001b, 2005). The ability of large non-penetrating impacts to produce voluminous distant secondary populations (McEwen et al. 2005; McEwen and Bierhaus 2006) is not in doubt, but it is also true that the dynamics of those populations are not yet fully understood (Ivanov 2006; Werner et al. 2006). If all of Europa's ≈10 million secondary craters (mapped and inferred: Bierhaus et al. 2005) were produced by the estimated 50–70 primary craters >10 km (mapped and inferred: Bierhaus 2004), then the ratio of secondary to primary craters would be $\approx 2 \times 10^5$ to 1, implying unexpectedly efficient ejecta production (Bierhaus et al. 2005). Such high production rates are not impossible: but measurements and calculations indicate that ejecta production on Europa at larger impact sizes is in fact *less* efficient, because of the involvement of liquid substrate (Moore et al. 1998). Taking into account the reduced production of secondaries by non-penetrating impacts that have been affected by underlying fluid, there is room in the secondary crater population estimates for a contribution from a greater number of impactors.

Additionally, although calculations permit that the non-penetrating impact craters might have produced sufficient ejecta to make all the known small craters (Bierhaus et al. 2001b), those same results also admit the interpretation that there are more secondary craters than can be accounted for by the known primary impacts. The estimated ratio of M_{ej} (secondary-forming ejecta likely to have been produced by the primary craters) to M_{re} (mass required to form the mapped small craters) ranges from 0.03–1.7 (Bierhaus et al. 2001b). Values less than 0.5 would mean that the ejected mass from large primary craters is insufficient to account for 50% of the measured small craters: i.e., if the true value for M_{ej} to M_{re} is between 0.03 and 0.5—a third of the estimated range—then there is an excess of secondary craters relative to known primaries. It follows that the calculated ratios permit—and might even require—an additional population of primary impactors. There are many uncertainties in this calculation, as the authors carefully note (Bierhaus et al. 2001b): we do not know the target properties, the ejection angles, or the specific distances between primary and secondary craters. But the results do tell us that there are enough small craters on Europa to permit the possibility of a larger population of primary impact sites.

Finally, Europan secondary craters—unlike the generally elliptical secondary craters on the Moon and Mars (Schultz 1972; Pike and Wilhelms 1978; Schultz and Singer 1980; McEwen et al. 2005)—are commonly circular. Craters in ice have low ellipticity (length/width <1.1) for impact angles 70–90° from the surface, becoming more elliptical (length/width 1.1–1.4) as angles decrease below 60° (Grey et al. 2002). Thus the circularity of Europa's secondary craters suggests generally steep trajectories, such as would result from impact into a low-viscosity or liquid water target (Schultz and Singer 1980; Gault and Sonett 1982; Schultz and Gault 1985; and references therein), and is consistent with ejecta being produced and deposited closer to the primary site, rather than necessarily undergoing long flight paths and distant travel. It is possible, therefore, that some of the secondary craters thousands of km distant from large craters may be the result of high-angle ejection from more proximal (as yet unmapped) penetrating-impact sites.

SPATIAL DISTRIBUTION OF CRATERS AND CHAOS

Spatial analysis of chaos and crater locations on Europa is complicated, for three reasons: first, because of the small number of large primary craters preserved on Europa, which makes the statistics of distribution challenging; second, because only about 15% of the satellite's surface has been imaged at 250 m/pixel or better; and third, because diverse lines of evidence indicate that the ice shell has been subject to non-synchronous rotation throughout its recorded geologic history (Geissler et al. 1998; Greenberg et al. 2002; Kattenhorn 2002; Figueredo and Greeley 2003; Hurford et al. 2007). So our analysis here is not conclusive, but represents a set of observations from which to move forward.

A synchronously rotating satellite is expected to show strongly asymmetric heliocentric-comet crater distributions, with a factor of order 40 difference in impact rates between the apex and antapex (Zahnle et al. 2003). That Europa's large craters do not show this distribution may be due to non-synchronous rotation or to the statistics of small numbers (Zahnle et al. 2001). In fact 75% of Europa's large craters are concentrated in the southern hemisphere, and more than half are within 30° of the equator. This distribution, while statistically significant, has no meaning in terms of impact dynamics: it is either a statistical artefact, or the consequence of surface reorganization by Europan tectonics and nonsynchronous rotation.

The distribution of chaos areas is likewise both interesting and puzzling, and has also doubtless been subject to rotational effects. Chaos areas are distributed across the body, but of the seven very large chaos regions (≈500–1500 km in longitudinal extent; see map in Doggett et al. 2007), six are concentrated at the apex and antapex, and centered on the equator. Smaller chaos areas in the equatorial regions tend to be clustered, and also tend to concentrate close to the large chaos regions (Spaun 2002; Spaun et al. 2004). If chaos terrain can be formed by impact, then the very large chaos regions might possibly represent the sites of very large impacts, and chaos areas clustered near them might represent secondary sites; but image coverage is not adequate to test this hypothesis.

In cases where the stratigraphic relationships can be tested, craters are generally younger than nearby chaos areas.

A number of craters directly overlie chaos terrain (e.g., Brigid, Amergin, and Manannán: Figueredo and Greeley 2004; Moore et al. 2001), implying crustal thickening prior to crater formation. In contrast, no known craters are directly overprinted by chaos terrain, and chaos areas rarely demonstrably post-date adjacent craters (for one example, see Kadel et al. 2000). As craters are generally the youngest features on Europa—few showing any signs of tectonic modification—it may be that there has been a secular shift from penetration-dominated to crater-dominated impact dynamics. This would be consistent with a progressive thickening of Europa's cryosphere (Figueredo and Greeley 2004).

We are currently mapping Galileo imagery to determine the spatial distribution of chaos in areas distant from the very large chaos regions and compare it to the spatial distribution of craters; and also to further analyse the relationship between the few very large chaos regions and the myriad smaller chaos areas. Unfortunately, we cannot make meaningful predictions about the expected distribution of chaos areas in the framework of the impact-chaos hypothesis, because even the large primary craters do not conform to the spatial distribution expected from known impactor populations (Schenk et al. 2004). To further frustrate matters, the incomplete medium-resolution imaging of Europa means that it is not possible to fully analyse the chaos areas' distribution, especially with respect to the very large chaos regions, which are themselves incompletely mapped (Doggett et al. 2007).

WHY IS THERE OVERLAP IN CHAOS AND CRATER SIZES?

If the crust of Europa is variable in thickness (Billings and Kattenhorn 2005; Nimmo et al. 2005), then we expect four things. First, there will be a lower limit on the size of penetrating impacts, given by the minimum crust thickness. Second, there will be an upper limit on crater size, because there is some critical impact size or energy—let's call it the ÜberPenetrator—that can overcome the thickest crust and will always penetrate. Third, there will be a range of impactor sizes for which there is a probability of either crater formation or penetration, depending on whether the impacted crust is thick or thin. Fourth, there will be a range of both crater and chaos morphologies for a given impactor energy (i.e., equivalent-bolide features), depending on the thickness of the impacted ice.

The first expectation is met by the relative size distributions of craters and chaos. Craters—which make up only 23% of the total population of craters+chaos—dominate the small-size end of the distribution, whereas chaos areas are most numerous at larger diameters (Table 3). There are many thousands of tiny craters (Bierhaus et al. 2001b, 2005), but no chaos areas <2 km diameter (Riley et al. 2000; Spaun et al. 2002, 2004; Ong 2004). The lower limit for impact-related chaos areas places a lower limit on local crustal thickness, as the smallest impactors can never penetrate. This could be quantified by hydrocode modelling, but is probably on the order of several hundred metres.

Table 3. Proportions of craters and chaos at different size ranges, showing that craters dominate at small sizes, but that chaos areas become much more numerous at larger diameters.

Size range (km diameter)	Craters (N = 300)	Chaos areas (N = 1002)	Chaos areas as % of features in size range
1–2	>200	1	0.5
2–4	62	37	37
4–8	21	326	94
8–40	17	623	97
40–100	0	15	100

In accordance with the second expectation, there are no craters larger than Tyre and Callanish (≈30–45 km) (Moore et al. 2001; Schenk et al. 2004). The lack of larger impact features has generally been ascribed to the youth of Europa's surface (e.g., Schenk et al. 2004), but it's also conceivable that Tyre and Callanish are the largest possible non-penetrating impacts—that 45 km is an upper limit on crater size—and that larger events always breach the crust. The fact that both Tyre and Callanish represent incipient penetration (Moore et al. 1998, 2001; Kadel et al. 2000; Schenk et al. 2004) supports this hypothesis. The maximum crater size may be controlled by the maximum crust thickness, such that larger impactors—ÜberPenetrators—will always penetrate the crust, forming second- or third-order impact features, possibly represented by large chaos areas such as Thera.

Consistent with the third expectation, craters and chaos overlap in the size range 2–40 km. Most of the overlap is actually concentrated in a much narrower size range: of the overlapping craters, 62% are 2–4 km, and 83% are 2–8 km in diameter. Within the zone of overlap, the relative proportions change: the percentage of chaos areas increases with increasing diameter, as the number of craters decreases (Table 3). At diameters greater than 8 km, the number of craters decreases drastically relative to chaos areas: in the range 8–40 km, there are only 17 known craters, compared with 623 chaos areas. At diameters greater than 40 km, only chaos areas are found. This is consistent with the hypothesis that the non-penetrating craters are formed by lower-energy events—less likely to penetrate—and that chaos areas are generated by more energetic impact events, with a higher penetration probability.

The fourth expectation, that chaos and craters should both show a range of morphology for a given size, is also met. For instance, Thera (80 km) is angular and raft-dense (platy chaos of Greeley et al. 2000), whereas Murias Chaos (95 km) is circular and raft-poor (knobby chaos of Greeley et al. 2000). Narberth Chaos and Arran Chaos (Fig. 1) provide a smaller scale example. Craters likewise show substantial variability (Moore et al. 2001). Pwyll and Manannán are very

Table 4. Rough estimates of the possible relationship between impactor size and chaos area. Calculations used the crater-scaling equations in Zahnle et al. (2003). See text for methods and caveats. Some large Europan craters are included for comparison.

Figure	Feature name	Measured area (km^2)	Equivalent circle diameter (km)	Corresponding transient crater diameter (km)	Comet diameter (km, 1.1 g/cm^3)	Comet diameter (km, 0.6 g/cm^3)
1b	None	3	2	2	0.1	0.1
1b	None	7	3	2	0.1	0.1
1f	None	64	9	6	0.3	0.3
1d	Arran Chaos	201	16	10	0.5	0.6
1a	Narberth Chaos	227	17	11	0.5	0.7
1e	Rathmore Chaos	1725	47	27	1.7	2.2
1g	Thera Macula	4764	78	42	3.0	3.8
1c	Murias Chaos	7154	95	51	3.7	4.8
	Craters:					
	Amergin		15	10	0.5	0.6
	Manannán		22	14	0.7	0.9
	Pwyll		24	15	0.8	1.0
	Callanish		38	23	1.3	1.7
	Tyre		44	26	1.5	2.0

close in size (24 and 22 km diameter, respectively), but have very different morphologies; likewise, Gráinne (14 km) has a central peak, but Math and Rhiannon (14 and 15 km, respectively) do not. Tegid and Taliesin (both ≈28 km, thus close in size to Pwyll) may be Tyre-like multi-ring features (Turtle and Phillips 1997; Moore et al. 2001).

The overlap in chaos and crater sizes is consistent with and in fact predicted by the impact penetration hypothesis in the context of variable crust thickness on Europa. Small impactors will always form craters; very large impactors will always penetrate; and intermediate impactors may either penetrate or not, depending on crust thickness. The crust thickness variation may be spatial: impactors of the same magnitude and age might have different impact outcomes in different areas. It might also be secular: impactor sizes that penetrated the crust in the past might, in more recent times, be more likely to form craters. It seems likely, however, that there is an absolute upper size for non-penetrating impacts, given by the maximum ice thickness.

What Size Impactor, What Ice Thickness?

Using an uncomfortable number of assumptions, but to provide a first-approximation look at relationships between chaos size, impactor diameter, and ice thickness, we calculated hypothetical impactor sizes for selected chaos areas using Zahnle et al. (2003) crater-scaling equations (Table 4). In this back-of-the-envelope approach, we took chaos diameter as equivalent to final crater diameter, and used 2.5 km as the transition value (per Zahnle et al. 2003) to estimate the transient hole size. These assumptions are gross oversimplifications at best, both because the physics of hole creation is different for craters and full penetration, so the scaling relationships are bound to be different; and also because varying ice thickness is bound to affect the impact dynamics in fundamental ways. But they provide a place to start, and we present the calculations as a rough first cut. We applied impactor densities of 1.1 and 0.6 g/cm^3 to facilitate comparison with the results of Turtle and Pierazzo (2001), and used the average impact velocity at Europa (26.5 km/s: Zahnle et al. 2003).

We can combine the data in Table 2 with published hydrocode modelling to begin thinking about the interactions between impactors and crust at different crust thicknesses. A 1 km impactor at average velocity can penetrate ice >5 km thick (Turtle and Pierazzo 2001); so a Callanish-scale impactor could potentially produce a Rathmore-type chaos area (Fig. 1e) if ice thickness were 5 km or less at the time of impact. An Amergin-size impactor (Table 4) might produce a Arran- or Narberth-type chaos (Figs. 1a–d) in ice up to 4 km thick (based on modeling by Turtle and Pierazzo 2001). For impactors 0.1 to 0.3 km in diameter to make chaos areas like those in Figs. 1B and 1F, substantially thinner ice would be required; but since local thicknesses of just few hundred m have been estimated (Billings and Kattenhorn 2005), this scenario is not impossible. At the other end of the scale, impactors of order 3–5 km would easily penetrate crust 5–10 km thick or more (Ivanov and Turtle 2001; Turtle and Pierazzo 2001); so hypothesizing the production of Thera Macula (Fig. 1g) and Murias Chaos (Fig. 1c) by such impactors is also reasonable.

What is the minimum size of the ÜberPenetrator? It depends on the thickness and strength of the ice crust, which is not well known; but there are clues in the crater record. If the largest impact structures known on Europa—Tyre and Callanish—are also the ones that most severely tested the limits of crustal resistance, it seems plausible that they represent the largest possible non-penetrating

structures. The 20 km-thick crust inferred to underlie them (Schenk 2002) may therefore be the thickest crust on Europa. Since Tyre and Callanish could be formed by comets of order 2 km diameter hitting at average velocity (Table 4; based on criteria in Zahnle et al. 2003), we propose that impactors somewhat larger than 2 km—say 2.5 km—are ÜberPenetrators.

At sizes less than the ÜberPenetrator impactors may penetrate or not, depending on the interplay between impact energy and local crust thickness. The potential for creation of a range of penetrating and non-penetrating equivalent-bolide features could explain why there are both craters and chaos areas in the ECD range 2–40 km. For example, a 1 km impactor in thick crust produces a ≈20 km first-order crater (Zahnle et al. 2003), of which there are two (Maeve and Manannán) mapped on Europa (Moore et al. 2001), and probably several more yet to be discovered (Bierhaus 2004). But the same impactor would penetrate 4 km thick crust (Turtle and Pierazzo 2001), possibly producing a 25 km chaos area (extrapolation from data on Table 4).

And how low can we go? The existence of a few chaos areas ≈4 km ECD suggests that very small impactors may penetrate in some instances; but the rarity of chaos this small—only 38 out of 1002 in our database—indicates that such thin crust is atypical at best. It is also possible that these very small chaos areas do not represent impact penetration but are formed by an endogenic process such as diapirism (Pappalardo et al. 1998; Spaun et al. 2004): there are no objective criteria yet for distinguishing between chaos areas formed by different mechanisms. Determining the size of the smallest possible penetrator depends on a better understanding of Europan crustal structure. The bottom line is that, whatever the cut-off for impact penetration, most small impactors will make craters, not holes.

THE SIZE-FREQUENCY DISTRIBUTION

The crater size-frequency distribution (SFD) for Europa shows a crater density dramatically different from those of its sister moons (Fig. 10). The impact production function at large diameters is presumed to be the essentially the same as that recorded on Ganymede and Callisto, but cannot be derived from the crater data because the small number of first-order craters—126 craters ≥1 km, and only 24 ≥ 10 km—is not a statistically significant population (Schenk et al. 2004). If chaos areas also represent impacts, however, then the database is substantially bigger—1280 features ≥1 km, and 432 ≥ 10 km—and the SFD of craters+chaos should approach a production population for Europa.

We can test this hypothesis by comparing the craters+chaos SFD to the Ganymede and Callisto production populations. To this end we measured craters and chaos areas from Galileo images with resolution <320 m/pixel covering ≈4.5 million km^2, i.e., almost 15% of Europa's surface. We measured only chaos areas that were completely contained within image or mosaic boundaries, so partial chaos areas at the edges of mosaics were not measured; and the seven very large chaos regions (as shown in Doggett et al. 2007) are likewise not included. We excluded chaos-like regions that did not have sharp boundaries for at least 2/3 of their perimeters, thus eliminating domes. We excluded all craters with diameters less than 1 km, as these are probably dominated by secondary impacts (Bierhaus et al. 2005); and also the near-field areas surrounding large first-order impacts such as Tyre and Callanish. The plotted size distribution (Fig. 10) therefore includes all identified primary craters >1 km diameter, and all chaos areas meeting the criteria given above.

The Size Distribution of Chaos Areas Shows a Maximum at about 7 km Diameter

Abundance of chaos increases with decreasing size down to about 40–80 km^2 (7–10 km ECD), below which size the number of chaos areas visible on Galileo images decreases dramatically with decreasing size (Riley et al. 2000; Spaun et al. 2000, 2002). But there is a question as to whether the decrease in abundance at small sizes is real (Pappalardo et al. 1998; Spaun et al. 1998, 1999; Spaun 2002), or whether it is an artefact of reduced recognizability given the image resolution limits (Greenberg et al. 1999; Hoppa et al. 1999; Riley et al. 2000). Mapping chaos on high-resolution images (30 m/pixel), covering 7400 km^2 of Europa's surface gave a greater density of small chaos areas in the high-resolution images than in medium-resolution ones (≈450/10^6 km^2 versus ≈200/10^6 km^2), suggesting that resolution was the dominant control on small chaos abundance, and that with higher-resolution images one would find increasing numbers of small chaos areas. But because the database from high-resolution images was very small—in total only 35 chaos areas <11 km ECD, and only about 15 that are <5 km ECD—the results were not statistically significant (Riley et al. 2000; Hoppa et al. 2001). On the other side of the argument, size-frequency analysis of features in 3700 km^2 of high-resolution imagery did not support increasing numbers of chaos areas at decreasing size (Spaun 2002), but again there were less than 40 features in the data set.

Without more high-resolution imagery from Europa it is not possible to solve this issue quantitatively. But we can make a strong qualitative argument that the observed peak in the chaos size distribution at 7–10 km ECD (Riley et al. 2000; Spaun et al. 2000, 2002) is real, because the existing high-resolution images show no evidence for chaos features below the limits of clear resolution. If the measured distribution peak were an artefact of image resolution, there should be large numbers of chaos areas hovering below the limits of resolution

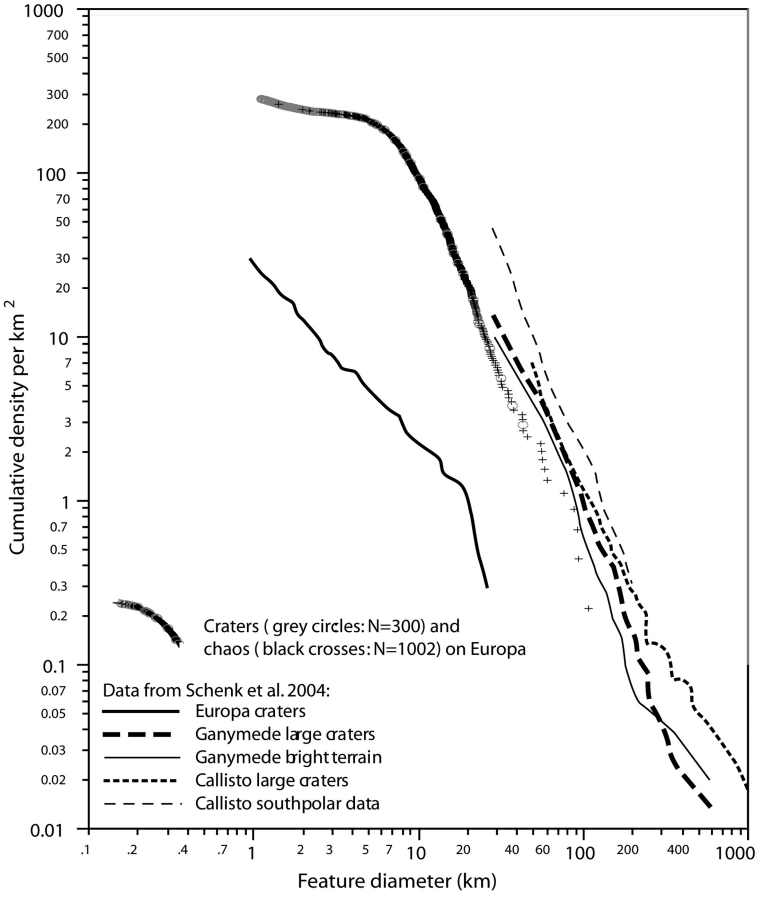

Fig. 10. Cumulative SFD for craters and chaos areas combined, shown in comparison to data (from Schenk et al. 2004) for craters on Europa, Ganymede, and Callisto. Graph constructed using methodology of Crater Analysis Techniques Working Group 1979). To reduce the influence of secondary crater populations, all Europan features with diameters less than 1 km were excluded, as were the secondary crater fields surrounding large impacts such as Tyre and Callanish. The dominance of craters (grey circles) at smaller diameters, and the transition to chaos areas (black crosses) at larger diameters (quantified in Table 3) can be seen on the graph, although data-point overlap blurs the details. In contrast to the anomalous pattern shown by Europan craters, the SFD for craters+chaos maps onto that for Ganymede and Callisto, and matches the predicted production function for impacts at Europa. For this analysis, we used raw diameters of craters and chaos areas (ECD); but we note that this is a first approximation as we do not actually know the relationship between the size of a penetrating impact feature and that of a non-penetrating crater of equivalent impact energy.

in all images; evidence from the images, however, indicates the opposite. Whereas the 200 m/pixel images show abundant ambiguous and fuzzy small features that turn out to be chaos areas when viewed at higher resolution (Greenberg et al. 1999; Riley et al. 2000; Hoppa et al. 2001), the 30–50 m/pixel images do not. The terrain at 30–50 m/pixel is clearly divisible into chaos, craters, bands, ridges, and troughs (terminology of Figueredo and Greeley 2004; Greeley et al. 2004). The definition is sharp, and the distinction between chaos and other terrain types is clear. Even the abundant tiny craters (diameter <150 m, 5 pixels across) are unmistakable. If there were a population of small chaos areas (diameter <7 km, or <23 pixels), the high-resolution images would contain hints, showing some kind of indistinct terrain; but this is not the case (see for example images archived at NASA's Galileo Legacy Site at http://solarsystem.nasa.gov/galileo/gallery/europa.cfm). So, we contend that existing chaos counts (Greenberg et al. 1999; Riley et al. 2000; Spaun 2002, and this study) do reflect reality, and that the absolute abundance of small chaos does decrease sharply with decreasing size, even when corrected for recognizability. We therefore use the chaos area counts along with crater data to examine the overall SFD for craters+chaos.

The Size-Frequency Distribution for Craters+Chaos Matches Production Functions for Ganymede and Callisto

The SFD for craters+chaos is markedly different from that for craters alone, and maps onto the crater SFDs of Ganymede and Callisto (Fig. 10). The match is very close at feature diameters >5 km, for which there are good body-wide data from all three satellites. At diameters <5 km the Europan SFD flattens, and then trends upward again at diameters <2.5 km. The flattening tendency has also been observed for the sister satellites at crater diameters 1–2.8 km (Ivanov and Basilevsky

2002); and the upturn at smallest diameters is consistent with Europan small-crater counts (Bierhaus et al. 2005)

R-plots display binned impact-size data relative to a power law of index −3—the "ideal" slope of a crater production function—such that an index −3 distribution would plot as a horizontal line (Crater Analysis Techniques Working Group 1979). These plots thus emphasize small-scale features of real size-frequency distributions and allow detailed comparison between different impact populations. Published R-plots for Europan craters (Fig. 11a) show little similarity to distributions from the nominal comparison populations of craters on younger regions of Ganymede and Callisto (Schenk et al. 2004), and there is also a marked discontinuity between the populations for small and large craters (Schenk et al. 2004; Bierhaus et al. 2005). The R-plot for Europan craters+chaos shows a much stronger similarity, in overall shape and in steepness, to crater distributions on the sister satellites (Fig. 11b).

The insights from the craters+chaos data also allow us to rationalize across the data gap between small and larger features. If we accept that the regional mapping from medium-resolution images probably undercounts features less than a few km diameter, then we can ignore the very low relative densities for craters 1–4 km, and smoothly connect the distributions for small and large features. Doing this—but recognizing that it is a first estimate, and that the data gap needs to be bridged by better regional imaging in the future—we produce a distribution that has a similar shape to the regional curve for Callisto, as well as values and slopes comparable to those on the Ganymede and Callisto young terrains (Fig. 11b).

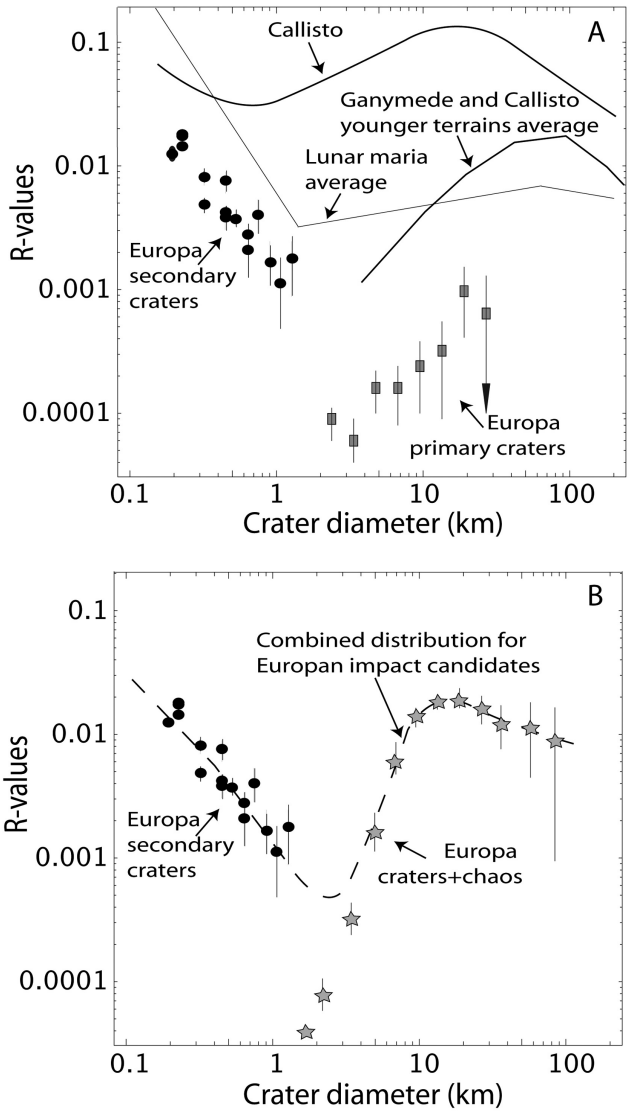

Fig. 11. a) Published data for Europa, showing the discontinuity between large (Schenk et al. 2004) and small (Bierhaus et al. 2005) crater populations. Curves for Callisto global, Ganymede and Callisto younger terrains (after Schenk et al. 2004) and lunar maria (after Bierhaus et al. 2005) included for comparison. b) Bierhaus et al. (2005) data for Europa small crater populations (dots) plotted with the combined size-frequency data for craters+chaos (stars). The craters+chaos curve at diameters 5–100 km is very similar to that of the young terrains on Ganymede and Callisto. The dashed line indicates our interpretation of the most likely global size-frequency distribution for Europa, taking into account that craters 2–5 km diameter are likely to be undercounted because of the 250 m/pixel resolution of the regional Galileo images. The vertical bars on the yellow stars represent errors on the estimates (Crater Analysis Techniques Working Group 1979)

Caveats

One fly in this ointment is that we do not know the relationship between the sizes of penetrating and non-penetrating impact features generated by equivalent impact energy. In our analysis, we used the raw diameters of craters and chaos areas (ECD), but we note that this has inherent inaccuracies. Second-order impact feature sizes may relate closely to the crater diameters of simple first-order craters; but because of the mechanics of wide-field fragmentation, third-order impact features may be substantially bigger than first-order craters produced by equivalent bolides (Fig. 6b). If chaos areas represent smaller impactors than craters of the same diameter, the craters+chaos SFD would shift leftward on Fig. 10. But as the experiment data are few and the scaling parameters still unquantified—and as there are some large chaos (e.g. Murias) that may be second order, and some much smaller that might be third-order (Fig. 1)—there is no universal correction that we can make to reconcile the two data sets. This analysis is therefore a first approximation.

A second point is that we include all counted chaos areas in the craters+chaos database. This carries the implicit assumption that all chaos areas are formed by impact, which we have no way of knowing. In the absence of objective criteria to assign different origins to different chaos areas, the only option is to treat all chaos areas equally; but we emphasize that the data set in Fig. 10 represents an end-member analysis, which may need to be revised when new data from Europa become available.

EUROPA'S SURFACE AGE

Europa's tectonically-reworked surface is clearly young. The resurfacing age, based on crater densities, is estimated at only 30–70 Ma (Zahnle et al. 2003). If chaos areas represent impact events, however, then the impact scar inventory is much increased, and the retention age of Europa's surface is correspondingly greater. The density of craters plus chaos is about $240/10^6$ km^2, given our count of 1280 features in $\approx 5 \times 10^6$ km^2 (Ong 2004). If we assume that all mappable chaos areas are caused by impact, then Zahnle et al.'s (2003) cratering rate of 5×10^7 craters (diameter ≥ 1km) km^2 Ma^{-1}, yields a nominal surface age of about 480 Ma. Incorporating Zahnle et al.'s factor of 3 uncertainty estimate in the rate calculations, the age bracket is 160–1440 Ma. Because we are including all counted chaos in this calculation, without knowing what proportion is impact related, this is clearly an upper limit on the resurfacing age. Although greater than current estimates (Schenk et al. 2004), this age is still very young by solar system standards: the nominal age of ≈500 Ma is less, for example, than the 700 Myr weighted average age of the Earth's surface.

CONCLUSIONS AND DIRECTIONS FOR FURTHER WORK

The small-scale experiments reported here provide an initial look at penetrating-impact behavior. Explosions in ice over water generate comparable features, and have also been compared with chaos areas (Billings and Kattenhorn 2003; Billings 2004). Hypervelocity equivalence is suggested by limited hypervelocity data at 2.5–6.2 km/s, which produced similar results: a simple hole at lower impact energy and full fragmentation at higher (Croft 1981; Croft, unpublished data; Scheider and Cox 2007). These are strength-regime experiments, but the data plot on established scaling trends established for solid-target impact outcomes (Ong 2004); and by analogy with established work (e.g., Holsapple 1993; Shrine et al. 2000), may provide some insights into behavior at planetary scales.

Europa's surface may therefore preserve a more interesting and varied impact record than previously recognized, on which individual impact outcomes are driven by the interplay between impactor size and local crust thickness. Small impacts, or impacts on thick crust, will form craters; impacts into thinner crust, or large ÜberPenetrators (>2.5 km diameter) that exceed the strength of Europa's thickest ice, may form chaos terrain. The great preponderance of chaos relative to craters—almost 9:1 at diameters 1 km and greater—suggests that Europan impact dynamics may have been dominated by crust penetration; but the lack of chaos areas that overprint craters implies that non-penetrating impacts are relatively more common in recent history.

The characteristics of Europan ejecta as recorded in the secondary crater population permit the existence of an additional set of impact sites. Rather than far-flung fragments from a few craters, some of Europa's secondaries may be clustered closer to their impact sites, represented by chaos areas. In the one place where we have sufficient high-resolution imagery to test this hypothesis—around Thera Macula (Fig. 7)—we find that secondary-crater distributions are correlated with distance from the chaos area. The data imply that higher-resolution imaging around Thera would reveal a mappable secondary crater field: like those around Tyre and Callanish and Pwyll, but at smaller scale. We emphasize the far smaller average size of the secondary craters around Thera, and the smaller density of craters/km^2 relative to first-order impacts like Pwyll and Tyre (Figs. 8 and 9).

The fact that most craters on Europa are undeformed (Figueredo and Greeley 2004), whereas many chaos areas have been modified (Riley et al. 2000, 2006) may indicate changes in crust thickness and consequent changes in impact dynamics through time. The zone of size overlap does suggest variations in crust thickness, but whether those changes are regional or secular, or both, we cannot yet say. The lower size limit on chaos areas indicates a lower limit on crustal thickness such that smaller impactors cannot penetrate. The existence of chaos areas just a few km in diameter suggests that at times and in places the crust is only a few 100 m thick; but their rarity indicates that such times and places are few and far between. Contrariwise, the lack of any craters larger than 40 km, and of craters with unambiguous solid-crust signatures >20 km—coupled with the abundance of big holes in the ground with diameters up to several hundred km—suggests that nowhere on Europa is the crust greater than a couple of 10s of km in thickness.

The combined craters+chaos record is comparable to measured SFDs at Ganymede and Callisto; and the resurfacing age of ≈500 Ma calculated on the basis of craters+chaos is compatible both with the extensive evidence for cryo-tectonic reworking, and with the lack of evidence for current or decadal-scale activity.

The results presented here are a first step toward understanding impacts into ice over fluid, but our data raise as many—if not more—questions than they answer. In contrast to solid-target impacts, for which there are abundant experimental data, very little is known about the physics of impacts into ice over liquid. These initial experiment data represent velocities in the hundreds of m/s range and the strength regime, so there are scaling questions to be addressed. In particular, we cannot make good inferences about the relationship between impactor size and chaos-area size, as the scaling relationships established for solid-target impacts will not apply; the estimates given in Table 4 are very rough indeed. Likewise, we do not know how the mechanisms of fracturing and block formation will change at planetary scale. Many puzzling aspects of the impact dynamics remain to be worked on: the physics of ejecta in layered solid-liquid targets, the role of waves and turbulence in the exposed liquid, the topographic response of freezing matrix, the nature

of outward-directed post-impact pressure, and the role of ice thickness variations, are all key aspects of that are not understood. But if we can quantify the geomorphology and physics of penetrating impacts we will have a tool for evaluating crustal thickness on Europa. For example, the ratio of 20 km craters to equivalent-bolide penetration features would be a rough measure of the proportions of crust thicker and thinner than 4 km. And the relationships between impactor flux rates and tectonic reworking of chaos areas and craters may allow us to estimate long-term deformation rates on Europa.

Although impact penetration explains many characteristics of chaos terrain—using a known energy source of the right magnitude, which can produce the appropriate geomorphology— impact is not necessarily a one-size-fits-all solution to the problem of chaos formation. Europa is an active, thin-skinned body and there are probably numerous ways in which its crust can be breached: domes and depressions that show partial disruption of the crust (Pappalardo et al. 1998; Greenberg et al. 2003) are clear evidence for this. The strange chaos area Thrace (Fig. 7) has flow-like features, and does not look like an impact site; and neither melt-through nor diapirism (e.g., Pappalardo et al. 1998; Collins et al. 2000; O'Brien et al. 2002) is negated by our model. We have also not addressed the very large regional chaos areas, such as that centered at 10 °S, 75 °W (Figueredo and Greeley 2004). These might represent very large ancient impacts, or may be formed by a different mechanism. We have insufficient constraints on ice thickness to evaluate the realistic lower limit on the size of penetrating impactors Europa-wide, because existing quantitative models rely on assumptions about ice parameters (Stevenson 2000), or are specific to a restricted area (Nimmo et al. 2003). Experiments and numerical modelling of penetrating impacts, and continued examination of existing Galileo images, may reveal criteria that distinguish between endogenic and exogenic formation of chaos; but future missions-returning higher resolution images for a larger proportion of the Europan surface-will be critical for answering these questions and understanding the genesis of chaos.

Acknowledgments—Many thanks to Steven K. Croft for sharing his unpublished hypervelocity impact data. Richard Greenberg and an anonymous reviewer provided constructive reviews that improved the paper, and we also thank Elizabeth Turtle, Beau Bierhaus, and Boris Ivanov for their thoughtful comments on earlier versions of this manuscript. The National Space Science Data Center and Dr. Michael J. S. Belton, the Galileo Project P. I., compiled and made available the Europa image data. Trent Hare of the USGS Astrogeology team sent georeferenced versions of the images and provided invaluable help with projections and area calculations. Financial support was provided by Williams College Department of Geosciences, the Bronfman Shared Overhead Fund, and NSF grant EAR 0415439 to RC.

Editorial Handling—Dr. Christian Koeberl

REFERENCES

Arakawa M. 1999. Collisional disruption of ice by high-velocity impact. *Icarus* 142:34–45.

Arakawa M., Leliwa-Kopystynski J., and Maeno N. 2002. Impact experiments on porous icy-silicate cylindrical blocks and the implication for disruption and accumulation of small icy bodies. *Icarus* 158:516–531.

Arakawa M., Maeno N., Higa M., Iijima Y.-I., and Kato M. 1995. Ejection velocity of ice impact fragments. *Icarus* 118:341–354.

Bierhaus B. 2004. Discovery that secondary craters dominate Europa's small crater population. Ph.D. thesis. University of Colorado, Boulder, CO, USA.

Bierhaus B. 2006. Crater signal-to-noise: Extracting Europa's small primary crater population, and what that means for the outer solar system small projectile population (abstract #6028). Workshop on Surface Ages and Histories: Issues in Planetary Chronology.

Bierhaus B., Chapman C. R., and Merline W. J. 2001a. On the clustering of Europa's small craters (abstract #1967). 32nd Lunar and Planetary Science Conference. CD-ROM.

Bierhaus E. B., Chapman C. R., and Merline W. J. 2005. Secondary craters on Europa and implications for cratered surfaces. *Nature* 437:1125–1127, doi:10.1038/nature04069.

Bierhaus E. B., Chapman C. R., Merline W. J., Brooks S. M., and Asphaug E. 2001b. Pwyll secondaries and other small craters on Europa. *Icarus* 153:264–276.

Billings S. E. 2004 Analysis of the ice shell of Jupiter's moon, Europa: Estimation of ice thickness and an examination of impact effects into a floating ice shell. M. S. thesis. University of Idaho, Moscow, USA.

Billings S. E. and Kattenhorn S. A. 2003. Comparison between terrestrial explosion crater morphology in floating ice and Europan chaos (abstract #1955). 34th Lunar and Planetary Science Conference. CD-ROM.

Billings S. E. and Kattenhorn S. A. 2005. The great thickness debate: Ice shell thickness models for Europa and comparisons with estimates based on flexure at ridges. *Icarus* 177:397–412, doi: 10.1016/j.icarus.2005.03.013

Collins G. C., Head J. W., Pappalardo R. T., and Spaun N. A. 2000. Evaluation of models for the formation of chaotic terrain on Europa. *Journal of Geophysical Research* 105:1709–1716.

Crater Analysis Techniques Working Group. 1979. Standard techniques for presentation and analysis of crater size-frequency data. *Icarus* 37:467–474.

Croft S. K. 1981. Hypervelocity impact craters in icy media. 12th Lunar and Planetary Science Conference. pp. 190–192.

Doggett T., Figueredo P., Greeley R., Hare T., Kolb E., Mullins K., Senske D., Tanaka K., and Weiser S. 2007. Global geologic map of Europa (abstract #2296). 38th Lunar and Planetary Science Conference. CD-ROM.

Fagents S., Greeley R., Sullivan R., Pappalardo R. T., Prockter L. M., and Team T. G. S. 2000. Cryomagmatic mechanisms for the formation of Rhadamanthys Linea, triple band margins, and other low-albedo features on Europa. *Icarus* 144:54–88. 10.1006/icar.1999.6254

Figueredo P. H., Chuang F. C., Rathbun J., Kirk R. L., and Greeley R. 2002. Geology and origin of Europa's mitten feature (Murias Chaos). *Journal of Geophysical Research* 107, doi:10.1029/ 2001JE001591.

Figueredo P. H. and Greeley R. 2000. Geologic mapping of the northern leading hemisphere of Europa from Galileo solid-state imaging data. *Journal of Geophysical Research* 105:22,629–22,646.

Figueredo P. H. and Greeley R. 2003. The emerging resurfacing history of Europa from pole-to-pole geologic mapping (abstract #1017). 34th Lunar and Planetary Science Conference. CD-ROM.

Figueredo P. H. and Greeley R. 2004. Resurfacing history of Europa from pole-to-pole geological mapping. *Icarus* 167:287–312.

Gault D. E. and Sonett C. P. 1982. Laboratory simulation of pelagic asteroidal impact: Atmospheric injection, benthic topography, and the surface wave radiation field. In *Geological implications of impacts of large asteroids and comets on the Earth*, edited by Silver L. T. and Schultz P. H. GSA Special Paper 190. Boulder: Geological Society of America. pp. 69–92.

Geissler P. E., Greenberg R., Hoppa G., Helfenstein P., McEwen A. S., Pappalardo R. T., Tufts B. R., Ockert-Bell M., Sullivan R., Greeley R., Belton M. J. S., Denk T., Clark B., Burns J., Veverka J., and Team G. I. 1998. Evidence for non-synchronous rotation of Europa. *Nature* 391:368–371.

Goodman J. C., Collins G. C., Marshall J., and Pierrhumbert R. 2004. Hydrothermal plume dynamics on Europa: Implications for chaos formation. *Journal of Geophysical Research* 109, doi: 10.1029/2003JE002073.

Greeley R., Chyba C. F., Head J. W., McCord T. B., McKinnon W. B., Pappalardo R. T., and Figueredo P. H. 2004. Geology of Europa. In *Jupiter: The planet, satellites and magnetosphere*, edited by Bagenal F., Dowling T., McKinnon W., Dowling T. E., and McKinnon W. B. Cambridge: Cambridge University Press. pp. 329–362.

Greeley R., Figueredo P. H., Williams D. A., Chuang F. C., Klemaszewsky J. E., Kadel S. D., Prockter L. M., Pappalardo R. T., Head J. W., Collins G. C., Spaun N. A., Sullivan R., Moore J. M., Senske D. A., Tufts R., Johnson T. V., Belton M. J. S., and Tanaka K. L. 2000. Geologic mapping of Europa. *Journal of Geophysical Research* 105:22,559–22,578.

Greeley R., Sullivan R., Klemaszewsky J. E., Homan K., Head J. W., Pappalardo R. T., Veverka J., Clark B. E., Johnson T. V., Klaasen K. P., Belton M. J. S., Moore J. M., Asphaug E., Carr M. H., Neukum G., Denk T., Chapman C. R., Pilcher C. B., Geissler P. E., Greenberg R., and Tufts R. 1998. Europa: Initial Galileo geological observations. *Icarus* 135:4–24.

Greenberg R. 2005. *Europa—the ocean moon*. Berlin: Springer-Praxis. 380 p.

Greenberg R. and Geissler P. 2002. Europa's dynamic icy crust. *Meteoritics & Planetary Science* 37:1685–1710.

Greenberg R., Geissler P., Hoppa G., and Tufts B. R. 2002. Tidal-tectonic processes and their implications for the character of Europa's icy crust. *Reviews of Geophysics* 40, doi:10.1029/2000RG000096.

Greenberg R., Hoppa G., Tufts B. R., Geissler P., and Riley J. 1999. Chaos on Europa. *Icarus* 141:263–286.

Greenberg R., Leake M. A., Hoppa G. V., and Tufts B. R. 2003. Pits and uplifts on Europa. *Icarus* 161:102–126.

Grey I. D. S. and Burchell M. J. 2003. Hypervelocity impact cratering on water ice targets at temperatures ranging from 100 K to 253 K. *Journal of Geophysical Research* 108:6:1–6:8.

Grey I. D. S., Burchell M. J., and Shrine N. R. G. 2002. Scaling of hypervelocity impact craters in ice with impact angle. *Journal of Geophysical Research* 107, doi:10.1029/2001JE001525, 2002.

Holsapple K. A. 1993. The scaling of impact processes in planetary sciences. *Annual Review of Earth and Planetary Science* 21:333–373.

Hoppa G., Tufts B. R., Greenberg R., and Geissler P. 1999. Formation of cycloidal features on Europa. *Science* 285:1899–1903.

Hoppa G. V., Greenberg R., Riley J., and Tufts R. 2001. Observational selection effects in Europa image data: Identification of chaotic terrain. *Icarus* 151:181–189.

Hurford T. A., Sarid A., and Greenberg R. 2007. Cycloidal cracks on Europa: Improved modelling and non-synchronous rotation. *Icarus* 186:218–233.

Ivanov B. A. 2006. Earth/Moon impact rate comparison: Searching constraints for lunar secondary/primary cratering proportion. *Icarus* 183:504–507, doi:10.1016/j.icarus.2006.04.004.

Ivanov B. A. and Basilevsky A. T. 2002. Morphology and size-frequency distribution of kilometer-scale impact craters on Callisto and Ganymede derived from Galileo data. *Solar System Research* 36:447–457.

Ivanov B. A. and Turtle E. P. 2001. Penetration of the ice crust on Europa during impact cratering: A lower limit for ice thickness (abstract #1013). 4th Lunar and Planetary Laboratory Conference.

Kadel S. D., Chuang F. C., Greeley R., Moore J. M., and Team G. S. 2000. Geological history of the Tyre region of Europa: A regional perspective on Europan surface features and ice thickness. *Journal of Geophysical Research* 105:22,657–22,669.

Kato M., Iijima Y.-I., Arakawa M., Okimura Y., Fujimura A., Maeno N., and Mizutani H. 1995. Ice-on-ice impact experiments. *Icarus* 113:423–441.

Kattenhorn S. A. 2002. Nonsynchronous rotation evidence and fracture history in the Brigh Plains region, Europa. *Icarus* 157: 490–506.

Lange M. A. and Ahrens T. J. 1981. Fragmentation of ice by low-velocity impact.Proceedings, 12th Lunar and Planetary Science Conference. pp. 1667–1687.

Lide D. R. 2002. *Handbook of chemistry and physics*. Boca Raton: CRC Press. 2640 p.

McEwen A. S. and Bierhaus E. B. 2006. The importance of secondary cratering to age constraints on planetary surfaces. *Annual Review of Earth and Planetary Science* 34:535–567, doi: 10.1146/annurev.earth34.031405125018.

McEwen A. S., Preblich B. S., Turtle E. P., Artemieva N. A., Golombek M. P., Hurst M., Kirk R. L., Burr D. M., and Christensen P. R. 2005. The rayed crater Zunil and interpretations of small impact craters on Mars. *Icarus* 176:351–381.

McKinnon W. B. 1999. Convective instability in Europa's floating ice shell. *Geophysical Research Letters* 26:951–954.

Mitri G. and Showman A. P. 2005. Convective-conductive transitions and sensitivity of a convecting ice shell to perturbations in heat flux and tidal-heating rate: Implications for Europa. *Icarus* 177: 447–460.

Moore J. M., Asphaug E., Belton M. J. S., Bierhaus E. B., Breneman H. H., Brooks S. M., Chapman C. R., Chuang F. C., Collins G. C., Giese B., Greeley R., Head J. W., Kadel S. D., Klaasen K. P., and Klemaszewsky J. E. 2001. Impact features on Europa: Results of the Galileo Europa Mission (GEM). *Icarus* 151:93–111.

Moore J. M., Asphaug E., Sullivan R. J., Klemaszewsky J. E., Bender K. C., Greeley R., Geissler P. E., McEwen A. S., Turtle E. P., Phillips C. B., Tufts B. R., Head J. W., Pappalardo R. T., Jones K. B., Chapman C. R., Belton M. J. S., Kirk R. L., and Morrison D. 1998. Large impact features on Europa: results of the Galileo nominal mission. *Icarus* 135:127–145.

Nimmo F. 2004. Non-Newtonian topographic relaxation on Europa. *Icarus* 168:205–208.

Nimmo F. and Giese B. 2005. Thermal and topographic tests of Europa chaos formation from Galileo E15 observations. *Icarus* 177:327–340, doi:10.1016/j.icarus.2004.10.034.

Nimmo F., Giese B., and Pappalardo R. T. 2003. Estimates of Europa's ice shell thickness from elastically-supported topography. *Geophysical Research Letters* 30, doi:10.1029/2002GL016660.

Nimmo F., Prockter L. M., and Schenk P. 2005. Europa's icy shell: Past and present state, and future exploration. *Icarus* 177:293–296.

O'Brien D. P., Geissler P., and Greenberg R. 2002. A melt-through model for chaos formation on Europa. *Icarus* 156:152–161.

Ong L. C. F. 2004 What lies beneath the surface? Europa's icy enigma. B. A. thesis. Williams College, Williamstown, MA, USA. http://library.williams.edu/theses/pdf.php?id=93.

Pappalardo R. T. and Barr A. C. 2004. The origin of domes on Europa: The role of thermally induced compositional diapirism. *Geophysical Research Letters* 31, doi:10.1029/2003GL019202.

Pappalardo R. T., Belton M. J. S., Breneman H. H., Carr M. H., Chapman C. R., Collins G. C., Denk T., Fagents S., Geissler P. E., Giese B., Greeley R., Greenberg R., Head J. W., Helfenstein P., Hoppa G., Kadel S. D., Klaasen K. P., Klemaszewsky J. E., Magee K. P., McEwen A. S., Moore J. M., Neukum G., Phillips C. B., Prockter L. M., Schubert G., Senske D. A., Sullivan R. J., Tufts B. R., Turtle E. P., Wagner R., and Williams K. K. 1999. Does Europa have a subsurface ocean? Evaluation of the geological evidence. *Journal of Geophysical Research* 104: 24,015–24,055.

Pappalardo R. T., Head J. W., Greeley R., Sullivan R. J., Pilcher C. B., Schubert G., Moore W. B., Carr M. H., Moore J. M., and Belton M. J. S. 1998. Geological evidence for solid-state convection in Europa's ice shell. *Nature* 391:365–368.

Pierazzo E. and Melosh H. J. 2000. Understanding oblique impacts from experiments, observations, and modelling. *Annual Review of Earth and Planetary Science* 28:141–167.

Pike R. J. and Wilhelms D. E. 1978. Secondary-impact craters on the Moon: Topographic form and geologic process (abstract). 9th Lunar and Planetary Science Conference. pp. 907–909.

Riley J., Greenberg R., and Sarid A. 2006. Europa's South Pole Region: A sequential reconstruction of surface modification processes. *Earth and Planetary Science Letters* 248:808–821.

Riley J., Hoppa G. V., Greenberg R., and Tufts R. 2000. Distribution of chaotic terrain on Europa. *Journal of Geophysical Research* 105:22,599–22,615.

Scheider K. C. and Cox R. 2007 Ice penetrating impacts: insights from hypervelocity impact experiments and Galileo image mapping of Europa (abstract #8034). Bridging the Gap II: Effects of Target Processes on the Impact Cratering Process.

Schenk P. M. 2002. Thickness constraints on the icy shells of the galilean satellites from a comparison of crater shapes. *Nature* 417:419–421.

Schenk P. M., Chapman C. R., Zahnle K., and Moore J. M. 2004. Ages and interiors: The cratering record of the Galilean satellites. In *Jupiter: The planet, satellites and magnetosphere*, edited by Bagenal F., Dowling T., McKinnon W., Dowling T. E. and McKinnon W. B. Cambridge: Cambridge University Press. pp. 427–456.

Schultz P. H. 1972. *Moon morphology: Interpretations based on Lunar Orbiter photography.* Austin: University of Texas Press. 626 p.

Schultz P. H. and Gault D. E. 1985. Clustered impacts: Experiments and implications. *Journal of Geophysical Research* 90:3701–3732.

Schultz P. H. and Singer J. 1980. A comparison of secondary craters on the Moon, Mercury, and Mars. Proceedings, 12th Lunar and Planetary Science Conference. pp. 2243–2259.

Shrine N. R. G., Burchell M. J., and Grey I. D. S. 2000. Velocity scaling of impact craters in water ice with relevance to cratering on icy planetary surfaces (abstract #1696). 31st Lunar and Planetary Science Conference. CD-ROM.

Spaun N. A. 2002 Chaos, lenticulae, and lineae on Europa: Implications for geological history, crustal thickness, and the presence of an ocean. Ph.D. thesis, Brown University, USA.

Spaun N. A., Head J. W., Collins G. C., Prockter L. M., and Pappalardo R. T. 1998. Conamara Chaos region, Europa: reconstruction of mobile polygonal ice blocks. *Geophysical Research Letters* 23:4277–4280.

Spaun N. A., Head J. W., and Pappalardo R. T. 2002. The spacing distances of chaos and lenticulae on Europa (abstract #1723). 33rd Lunar and Planetary Science Conference. CD-ROM.

Spaun N. A., Head J. W., and Pappalardo R. T. 2004. Europan chaos and lenticulae: a synthesis of size, spacing, and areal density analyses (abstract #1409). 35th Spaun N. A., Head J. W., Pappalardo R. T., and Team G. S. 2000 Analysis of chaos and lenticulae on the leading quadrant of Europa (abstract #1044). 31st Lunar and Planetary Science Conference. CD-ROM.

Stevenson D. J. 2000. Limits on the variation of thickness of Europa's ice shell (abstract #1431). 33rd Lunar and Planetary Science Conference. CD-ROM.

Tufts B. R. 1998 Lithospheric Displacement Features on Europa and their Interpretation. Ph.D. thesis, The University of Arizona, Tucson, AZ, USA.

Turtle E. P. 2004 What Europa's impact craters reveal: results of numerical simulations (abstract #7020). Workshop on Europa's Icy Shell: Past, Present, and Future.

Turtle E. P. and Ivanov B. A. 2002. Numerical simulations of impact crater excavation and collapse on Europa: Implications for ice thickness (abstract #1431). 33rd Lunar and Planetary Science Conference. CD-ROM.

Turtle E. P. and Phillips C. B. 1997. Multi-ring basins on Europa: Implications for subsurface structure. *Bulletin of the American Astronomical Society* 29:985.

Turtle E. P. and Pierazzo E. 2001. Thickness of a Europan ice shell from impact crater simulations. *Science* 294:1326–1328.

Weiss R., Wünnemann K., and Bahlburg H. 2006. Numerical modelling of generation, propagation and run-up of tsunamis caused by oceanic impacts: Model strategy and technical solutions. *Geophysical Journal International* 167:77–88, doi: 10.1111/j.1365-246X.2006.02889.x

Werner S. C., Ivanov B. A., and Neukum G. 2006 Mars: Secondary cratering-implications for age determination (abstract #6008). Workshop on Planetary Chronology.

Williams K. K. and Greeley R. 1998. Estimates of ice thickness in the Conamara Chaos region of Europa. *Geophysical Research Letters* 25:4273–4276.

Zahnle K., Dones L., and Levison H. 1998. Cratering rates on the Galilean satellites. *Icarus* 136:202–222.

Zahnle K., Schenk P., Levison H., and Dones L. 2003. Cratering rates in the outer solar system. *Icarus* 163:263–289.

Zahnle K., Schenk P., Sobieszczyk S., Dones L., and Levison H. 2001. Differential cratering of synchronously rotating satellites by ecliptic comets. *Icarus* 153. pp. 111–129.